

CONCURRENTLY COUPLED MULTISCALE MODELING
OF POLYMER NANOCOMPOSITES

by

SHIBO LI

SAMIT ROY, COMMITTEE CHAIR

VINU UNNIKRISHNAN

MARK BARKEY

GARY CHENG

JIALAI WANG

A DISSERTATION

Submitted in partial fulfillment of the requirements
for the degree of Doctor of Philosophy
in the Department of Aerospace Engineering and Mechanics
in the Graduate School of
The University of Alabama

TUSCALOOSA, ALABAMA

2016

Copyright Shibo Li 2016
ALL RIGHTS RESERVED

ABSTRACT

Embedded statistical coupling method (ESCM) was originally developed to provide computational efficiency, to decrease coupling complexities, and to avoid the need to discretize the continuum model to atomic scale resolution in concurrent multiscale modeling. ESCM scheme is relatively easy to implement within conventional FEM code and has been tested in standard solid lattice structures. However, this method encounters difficulties when being implemented for amorphous materials like polymers, due to the fact that they lack specific ordered lattice structure and atoms may not be covalently bonded with each other, which are the requirements of common coupling schemes. Therefore, a new approach needs to be developed to resolve this problem. In this paper, details of a modified ESCM approach for atomistic-continuum coupling developed to perform simulations of crack growth in polymers is presented. The presence of the continuum domain surrounding the MD region allows for the application of far field loading, and prevents stress wave reflections from the external boundary impinging back on the crack tip. In our approach, Material Point Method (MPM), which is a meshless particle-in-cell method based on Arbitrary Euler-Lagrange (ALE) scheme and has been proven to have good performance in large deformation problems, is used to model the continuum domain. It is concurrently coupled with molecular dynamics (MD), a widely used method in atomistic simulations, using a so-called handshake region. Anchor points, the equilibrium positions of the constrained particles, which are designed to transmit displacements and forces between nanoscale and macroscale model, are defined in the handshake region. A concurrently coupled

MPM-MD simulation of crack propagation inside a polymer is performed to verify this new coupling approach, thereby providing a better understanding of the fracture mechanisms at the nanoscale to predict the macro-scale fracture toughness of polymer system. Results are presented for concurrently coupled crack propagation simulation in a di-functional cross-linked thermoset polymer, EPON 862. The composite laminate open hole tension problem is also studied using concurrent multiscale approach by implementing micromechanics program MAC/GMC in FEA frame.

DEDICATION

This dissertation is dedicated to my family and friends who stood by me throughout the time taken to complete this research. In particular, to my parents who provided unconditional support and were extremely patient and encouraging through good and bad times.

LIST OF ABBREVIATIONS AND SYMBOLS

MPM	Material Point Method
MD	Molecular Dynamics
FEM	Finite Element Method
QC	Quasicontinuum
LEFM	Linear Elastic Fracture Mechanics
OPLS	Optimized Potential for Liquid Simulations
ReaxFF	Reactive Force Field
LAMMPS	Large-scale Atomic/Molecular Massively Parallel Simulator
ESCM	Embedded Statistic Coupling Method
IVC	Interface Volume Cell
SVC	Surface Volume Cell
DPD	Dissipative Particle Dynamics
J	J-integral
J_{Ic}	Critical Value of J-integral
K	Stress Intensity Factor
K_{Ic}	Fracture Toughness
σ_{th}	Theoretical material strength
a_c	Critical crack length

MOC	The Method of Cells
GMC	The Generalized Method of Cells
MAC/GMC	Micromechanics Analysis Code based on the Generalized Method of Cells
OHT	Open Hole Tension
CT	Compact Tension
p	Particle number
I	Node number
\mathbf{P}	Momentum
\mathbf{f}	Force
$N_I(\mathbf{x})$	Interpolation function for node I
$\chi_p(\mathbf{x})$	Particle shape/characteristic function
$\delta(\mathbf{x})$	Dirac delta function
\mathbf{F}	Deformation gradient tensor
VCCT	Virtual Crack Closure Technique
SERR	Strain Energy Release Rate
NRPC	Nano-particle Reinforced Polymer Composite

ACKNOWLEDGMENTS

I would first like to express my deep gratitude to my advisor, Dr. Samit Roy, for his constant guidance and support through the research for this dissertation. His patience and support helped me overcome many difficulties and finish this dissertation. I would like to thank Dr. Vinu Unnikrishnan for the long discussions that helped me sort out the technical details of my work. His knowledge and help were of great help in completing the simulations. I am grateful to Dr. Gary Cheng for his knowledge in molecular dynamics, his encouragement and practical advice. I would also like to thank Dr. Mark Barkey and Dr. Jialai Wang for serving on my dissertation committee and for their inputs in the preparation of this manuscript. I am thankful to the National Aeronautics and Space Administration (NASA) for the financial support for this research. I would like to thank Dr. Avinash Akepati, Mr. Abhishek Kumar and Mr. Pruthul Ravindranath for the many valuable discussions that helped me understand my research area better. I would also like to thank the members of my research group and friends in Tuscaloosa for their constant support and encouragement. Finally, I express my deep acknowledgments to my parents, who have always been a constant source of love, concern, support and strength all these years.

CONTENTS

ABSTRACT.....	ii
DEDICATION.....	iv
LIST OF ABBREVIATIONS AND SYMBOLS	v
ACKNOWLEDGMENTS	vii
LIST OF TABLES.....	xi
LIST OF FIGURES	xii
1. INTRODUCTION	1
2. CONTINUUM MODELING.....	11
2.1 Theoretical background	11
2.2 Explicit time integration	14
2.3 Mesh refinement	17
2.4 Crack modeling in MPM	18
2.5 Verification of MPM dynamics	21
2.6 Stress wave propagation in MPM.....	24
3 MOLECULAR DYNAMICS	27
3.1 Introduction.....	27
3.2 Numerical integration	28
3.3 Potential function	29
3.4 Ensembles	32

3.5 Atomistic J-Integral calculation	34
3.5.1 Linear elastic fracture mechanics.....	34
3.5.2 J-integral	36
3.5.3 Numerical atomistic J estimation.....	39
4 CONCURRENT MULTISCALE COUPLING SCHEME.....	42
4.1 Embedded Statistical coupling method.....	42
4.2 Anchor points.....	44
4.3 Modified ESCM coupling procedure.....	44
4.4 Model application: crack modeling in MD-MPM	48
4.5 Programming.....	51
5 RESULTS	54
5.1 Model benchmark: crack propagation of graphene	54
5.2 Crack propagation of cross-linking polymers.....	58
5.3 Problems and future work.....	60
6 HIERARCHICAL MULTISCALE SIMULATION OF OPEN HOLE TENSION TEST FOR A COMPOSITE LAMINATE USING MAC/GMC	61
6.1 Micro-scale modeling using MAC/GMC	61
6.2 Progressive failure modeling of delamination using cohesive zone in FEA.....	63
6.3 Fracture of open hole composite laminates	64
6.4 Three-dimensional ply-level analysis using finite element modeling	66
6.5 Case study: Simulation of an Open Hole Tension experiment using hierarchical multi-scale modeling	67
6.5.1 Case study 1: OHT simulation of laminate with [0/90] _s layup	68

6.5.2 Case study 2: OHT simulation of laminate with $[45/0/-45/90]_{2s}$ layup.....	73
6.6 Summary and discussion.....	80
REFERENCES	82

LIST OF TABLES

6.1 NRPC matrix properties.....	68
6.2 Fiber properties	68
6.3 Strength comparison of neat resin and 2wt% NGP	72
6-4 IM7 Fiber properties.....	74
6.5 Epon862 matrix properties.....	75
6.6 cohesive zone properties	75

LIST OF FIGURES

1.1 Compact tension fracture test results for baseline and nanographene reinforced EPON 862 epoxy specimens (at room temperature)	2
1.2 Length and time scale of multiscale mechanics.....	3
2.1 Lagrangian Material points distributed on a background Eulerian grid	12
2.2 Five-node linear element.....	17
2.3 Three level of refined meshes from transitioning	18
2.4 Schematic for determining strain energy release rate (SERR) in GIMP.....	18
2.5 MPM dynamics test case: A simply-supported bar with a single harmonic force	22
2.6 Case study: beam deflection vs. time.....	23
2.7 Information updating of material points and grid nodes.....	24
2.8 Wave propagation on a bar	25
2.9 Wave propagation of the MPM simulation.....	26
3.1 Three modes of fracture: (A) mode I: tensile opening; (B) mode II: in-plane shearing; and (C) mode III: out-of-plane shearing	35
3.2 Edge-cracked plate under uniform tension loading	36
3.3 Γ_ϵ and C_ϵ contour direction	38
3.4 J-integral contour and the Gaussian quadrature points	40
4.1 MPM-MD coupling system setup.....	45

4.2 Flowchart of MPM-MD coupling procedure	47
4.3 Crack propagation process flow chart.....	49
4.4 Crack begins to propagate into MD zone	50
4.5 Crack reinitiates on the GIMP zone and propagates through	51
4.6 Pseudo code for the Verlet::run() method for each step	53
5.1 MPM-MD coupling model configuration.....	55
5.2 Crack propagation in MD domain in a single graphene sheet	57
5.3 J-integral vs. time plot.....	58
5.4 Crack propagation in MD domain for EPON 862	59
6.1 RUC model for IM 7/NRPC composite.....	63
6.2 Three types of failure mechanisms of laminate ([50]).....	65
6.3 Micro-macro coupling (MAC-GMC/Abaqus).....	66
6.4 FEA model and boundary conditions	69
6.5 Damage prediction of [0/90] _s laminate (2.4% wt graphene).....	70
6.6 Average traction vs. strain plot (Neat resin and 2wt% graphene)	71
6.7 Micro and micro stress vs. strain plot of element on 0 °lamina (2wt% graphene).....	72
6.8 Micro and micro stress vs. strain plot of element on 90 °lamina (2w% graphene).....	73
6.9 Open hole tension specimen geometry	73
6.10 OHT FEA model and boundary conditions in laminate	76
6.11 IM7/ Reinforced EPON 862 OHT simulation-stress contour for individual lamina as a function of applied strain	78
6.12 (a) Load displacement plot for multiscale OHT simulation for various cases (b) Magnified view at load drop	79

CHAPTER 1

INTRODUCTION

Composites provide advantages over conventional material in the aspect of higher specific stiffness and strength, lower production cost, reduced maintenance cost and longer life cycle, which is due to its excellent resistance to corrosion, chemical attack and outdoor weathering in general cases as well. Polymer nanocomposites (PNC), defined as polymers having nanoparticles or nanofillers dispersed in the polymer matrix to produce materials with enhanced properties, have been studied for years and are implemented in industry increasingly over recent years. Unlike traditional filled polymer systems, relatively low dispersant loadings is required to achieve significant property improvements in nanocomposites and this feature make them excellent options for aerospace industry which pursuits lighter structure weight with higher strength .

Compact-tension (CT) tests were performed in this research to estimate the improvement of the enhanced nanocomposites quantitatively. A significant increase in peak failure load (by 141% and 190%) and fracture toughness (by 142% and 200%) over baseline specimens are observed at the same testing condition for EPON-862 epoxy enhanced with only 0.1wt% and 0.5wt% nano-graphene respectively [1]. The enhancement can be explained by the deflection of the crack due to the existence of graphene. Similar results of the improved properties of graphene epoxy are also published by Raifee *et al.* [12].

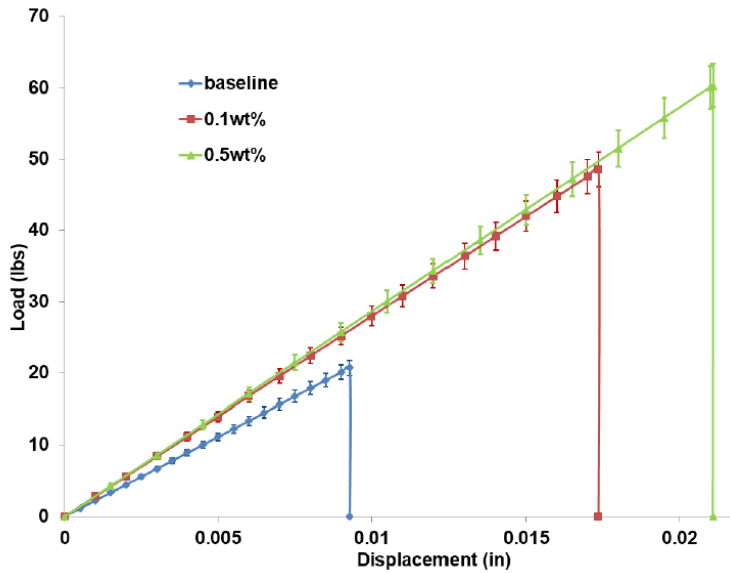


Figure 1.1 Compact tension fracture test results for baseline and nanographene reinforced EPON 862 epoxy specimens (at room temperature)

Studies in the range from nanoscale to macroscale have to be performed in order to better understand the local effect of nanoparticles on the mechanical properties of nanocomposites, such as, fracture toughness. However, for a typical nanoparticle reinforced composite, for example nanographene reinforced carbon fiber-polymer composite, both the length scale and the time scale which are needed to be concentrated on will be varying in a giant range, which can reach from nanometer (10^{-9} meter) to meters in length and from femtosecond (10^{-15} second) to second or even days and years, as depicted in Figure 1.2.

Challenges in the chemical and materials technologies lie in the requirement of the information for the dynamic properties of the atoms or particles. Experimental techniques can provide the information required, but usually are not able to capture the events at the atomistic scale, which has a unique spatial and time resolution compared with the macro scale. Therefore, multi-scale computational methods, such as Integrated Computational Materials Engineering

(ICME), which have been developed to bridge different time and length scales, enable us to better understand the atomistic scale events and obtain the knowledge to optimize our design and make use of the material in a much more effective way.

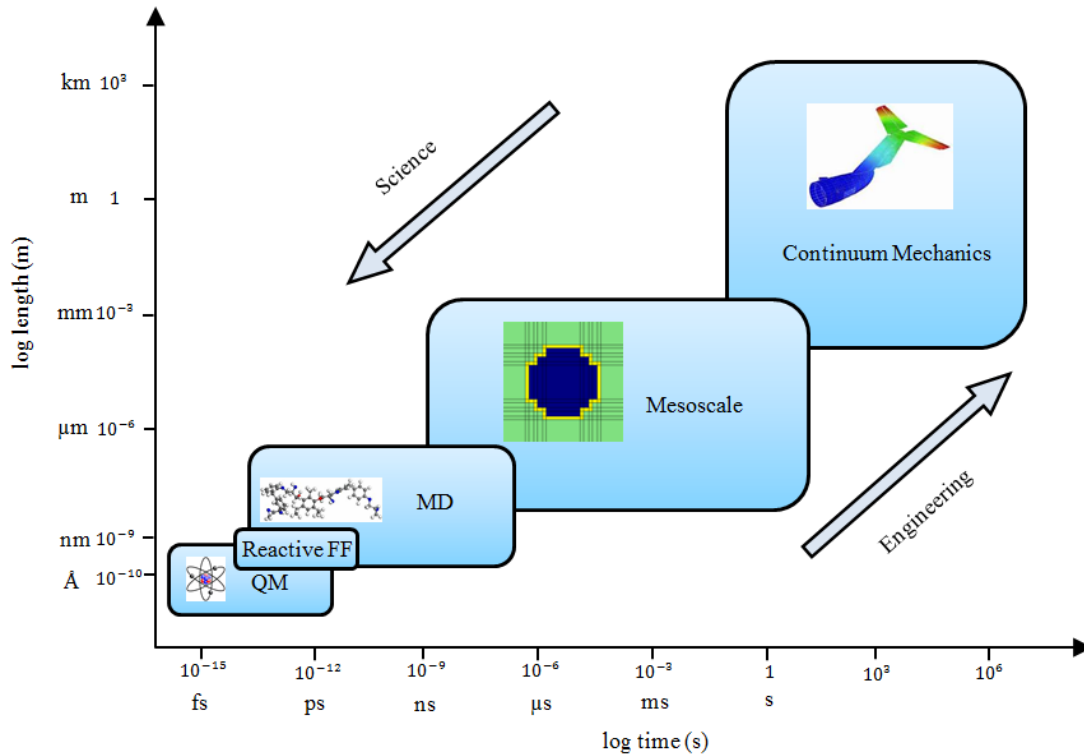


Figure 1.2 Length and time scale of multiscale mechanics

Continuum mechanics methods such as finite element method (FEM) provide an economical way to simulate macroscopic mechanical behavior of material. On the other hand, molecular dynamics (MD) makes it possible to find the properties of complex systems numerically using theoretical physics and provide a new perspective to our understanding of mechanics of material. Over the last decades, there has been a new realization that studying the nanoscale behavior is needed to understand failure and fracture behavior of materials, which also inspired people to

design materials from the bottom up. In recent years, numerous efforts have been directed towards modeling nanocomposites in order to better understand the reasons behind the mechanical properties enhancement with the addition of a few weight percent of nano-particles [1]. Nano-scale analysis is required in order to better understand the local effect of nanoparticles to the mechanical properties of the composite. However, atomistic modeling encounters increasing difficulties in computational cost as the system size increases. Multiscale modeling involving continuum mechanics and nanomechanics came into sight in the past few decades as it is considered computationally applicable to larger scale systems while providing information from different scales. Two main types of multiscale modeling, namely, the hierarchical and concurrent simulation schemes gained popularity with researchers as these allowed them to examine and understand small-scale phenomena using MD and macro-scale responses using continuum mechanics, and to overcome the problems of modeling relatively large material domains to capture continuum deformation field while maintaining atomic representations in localized areas. The hierarchical scheme sequentially isolates the mechanical system into different scales and the results will be converted to continuum responses by implementing averaging techniques. Concurrent multi-scale scheme displays a unique advantage over hierarchical approach in that it can connect local events at the nanoscale to stimuli from continuum scale, which is much larger in time and length scales, during real time simulation. Concurrent multiscale modeling can be used to obtain numerical solutions for extremely localized problems such as dislocations and crack propagation [2].

In recent years, numerous approaches have been proposed on concurrent multi-scale coupling of continuum mechanics and atomistic mechanics. The quasicontinuum (QC) method, proposed by Miller *et al.* [3], is formed based on atomistic description of the entire material model, which

is viewed as a finite element model. Several variants of the QC method have also been developed. For example, Knap and Ortiz [4] have proposed a form of QC method based on rep-atoms that bypass the distinction between atomistic and continuum domains. QC method requires the atoms to be coincident with the finite element nodes for accurate computation of the energy in the atomistic subdomain.

Alternately, Belytschko and Xiao [5] have developed the so-called bridging domain method in which the energies of the atomistic and continuum models are scaled in the overlapping domain. In order to enforce the kinematic constraints in the overlapping subdomain between the two scales, a Lagrange multiplier method is used. The bridging domain method is able to reduce spurious wave reflection at the interface by using energy descriptions of the system.

Saether *et al.* [6], proposed a statistical averaging approach to couple MD with FEM simulations and to overcome “finite-size artifact” problems, which are encountered in direct coupling methods. In their proposed embedded statistic coupling method (ESCM) scheme [6], interface volume cells (IVCs) are introduced to transfer information between FEM and MD while surface volume cells (SVCs) are formed to eliminate free edge effects, such as ghost forces, for the MD region.

However, most of the proposed multiscale methods are restricted to crystalline materials e.g. metals. For example, the use of the local harmonic (LH) approximation based on the Cauchy-Born rule as employed by Jones *et al.* [7] is not valid for an amorphous polymer with disorderly molecular configurations and random free-volume distributions. Recently, Roy *et al.* [8] applied Hardy’s methodology [9] to compute atomistic J-integral for a 10nm×10nm single nanographene platelet with a 2 nm center crack and compared it with results from linear elastic fracture mechanics (LEFM) predictions for isothermal crack initiation at 0 K and at 300 K using the

OPLS potential available in the MD software, LAMMPS [10]. In this context, Cheng and Sun [11] pointed out that the fracture toughness measured using critical stress intensity factor or energy release rate is crack size dependent because for a very small crack length the far field critical stress may exceed the theoretical strength of the material, giving rise to a transition from brittle fracture to ductile failure.

Recently, S.Pfaller *et al.* [12] developed an Arlequin-based method of coupling MD and FEM to simulate amorphous polymers and nanocomposites material. This new method introduces the so-called ‘anchor point’ which anchors onto the FEM elements and connects to an individual MD particle using harmonic potential. The anchor-point approach has to minimize perturbations on the MD system due to the newly added anchor points and form a good coupling connection by choosing appropriate stiffness value for the anchor. Moreover, to maintain the temperature of the MD region and simulate the periodic condition using non-periodic boundaries, the Dissipative Particle Dynamics (DPD), which is a stochastic approach, is applied to the boundary region.

In this dissertation, anchor point method is used as the coupling components of continuum and MD system. The mechanical variables like displacements and forces are transmitted through anchor points by implementing a statistical coupling approach, which is a modified form of ESCM.

Material Point Method (MPM) [16] is employed in this work to model the continuum domain due to its better performance in solving large deformation problems and the compatibility to couple with MD. In practice, a uniform grid can either be too computationally expensive or inaccurate depending on the mesh and the type of problem. Tan *et al.* [13] and Ma *et al.* [14] implemented the Structured Adaptive Mesh Refinement Application Infrastructure (SAMRAI) to

handle the multi-level grid information using MPM. Ma [15] proposed a mesh refinement scheme for Generalized Interpolation Material Point (GIMP) method based on regular grid by introducing an Influence Zone. Lian *et al.* proposed a tied interface grid material point method (TIGMPM) to solve problems of localized extreme deformation. In this dissertation, a classic MPM model with mesh refinement technique is applied.

S. H. Cheng and C. T. Sun [11] proved that the fracture toughness estimated by stress intensity factor or energy release rate is not a fixed material property but changing with the crack length, for the reason that the size of the K-dominance zone decreases as the crack length decreases and critical stress intensity factor K_{Ic} or critical energy release rate G_{Ic} cannot fully capture the fracture driving force if the singular stress is not dominant near the crack tip. From linear elastic fracture mechanics (LEFM), the critical crack length of a material at which its theoretical strength is exceeded under mode I loading can be estimated as

$$a_c = \frac{K_{Ic}^2}{\pi\sigma_{th}^2} = \frac{EG_{Ic}}{\pi\sigma_{th}^2} \quad (1)$$

where K_{Ic} is the mode I fracture toughness of the material, σ_{th} is the theoretical material strength, E is the material constant dependent on plane-strain or plane stress condition. From Eq.(1), we know that the critical crack length a_c has to be reached for the material to show the fracture behavior which can be predicted using continuum fracture mechanics. K_{Ic} and G_{Ic} cannot be considered as a constant when the size of the specimen is smaller than the critical length. If the criterion is satisfied, a clear crack may be observed and the fracture toughness can be calculated from continuum fracture mechanics; otherwise, a distributed damage may occur to the whole specimen rather than on the crack tip. The reason for this can be explained as the result of the continuum fracture mechanics derived from continuum models that adopt singular crack-tip

stress field represented by the stress intensity factor. The MPM-MD multiscale concurrent coupling approach is proposed to solve this problem, because, in this scheme, the continuum domain which is coupled with the MD domain can be enlarged to meet the critical crack length criterion can save the computational cost by using a small MD model.

Another way to perform the multiscale simulation is through micromechanics. The method of cells (MOC) is a micromechanical model introduced by Aboudi [33], and it is able to predict the overall behavior of different types of composites accurately by applying constituent properties. Explicit effective constitutive equations for the inelastic behavior of the matrix-reinforcement based composites can be obtained by making use of the method. In MOC, a periodic square array of fibers is represented as a unit cell consisting of four rectangular subcells. Properties of fiber and matrix are assigned to the subcells to model the composite material. The expansion coefficients can be obtained by using this approach, as well as the macro- and microscopic stresses and strains.

The generalized method of cells (GMC) [34] allows the repeating unit cell to be divided into an arbitrary number of subcells, to which phase properties are assigned. GMC also extends the modeling capability of MOC in the following aspect: thermomechanical response, variable fiber shapes, different fiber arrays, porosities/damage, and interfacial regions around inclusions. One advantage of GMC over other numerical techniques is that the full set of effective elastic properties of a composite can be calculated in one step instead of solving a number of boundary value problems with different boundary conditions. GMC has also been found to be more computationally efficient than finite element calculations for fiber reinforced composites (Aboudi 1996, Wilt 1995), since far fewer GMC subcells than finite elements are necessary to obtain the same degree of accuracy. The problem of discretization is also minimized since a regular

rectangular grid is used in GMC.

Bennett and Haberman [35] adopted the MOC analysis to establish a micromechanical approach. They proposed to unify the finite element method and the MOC to provide a practical tool for including micromechanical effects in structural calculations. Bednarczyk and Pindera [37] developed an analytical model based on the MOC and the classical lamination theory to investigate the effect of the matrix inelastic constitutive representation and the effect of nonuniform fiber distribution on the thermal expansion of unidirectional graphite/copper composites. Based on the GMC, NASA Glenn Research Center developed a micromechanics computer code, referred to as MAC/GMC (Micromechanics Analysis Code based on the Generalized Method of Cells), that has many user-friendly features and significant flexibility to predict the inelastic response of both continuous and discontinuous/woven multi-phase composites with arbitrary internal microstructures and reinforcement shapes. MAC/GMC accurately predicts the elastic and inelastic thermomechanical and piezo/magnetolectric response of multiphased materials including polymer-, ceramic-, and metal-matrix composites and laminates.

It should be noted that the multiscale implementations of GMC are spatially hierarchical for the reason that it explicitly homogenize and localize the fields at a given point. However, the approach is temporally concurrent because all the points are dealt with at once. The combination of hierarchical and concurrent multiscale frames has been called synergistic multiscale modeling [58].

In this dissertation, the anchor point method will be used to couple components between the continuum and MD systems. The continuum system used in this dissertation is not FEA, but the Material Point Method (MPM). The mechanical variables like displacements and forces will be

transmitted through anchor points by implementing a statistical coupling approach, which is modified from the ESCM approach 0. The remainder of the dissertation is organized as follows. Chapter 2 and 3 will describe the MPM and MD approaches, which are used in the multiscale scheme, respectively. Chapter 4 discusses the detailed coupling method proposed. Chapter 5 presents the numerical case of crack propagation in nanographene and in polymer nanocomposites to perform verification studies of the coupling approach, discussion, conclusions, and future work. Chapter 6 describes MAC/GMC, FEAMAC and their applications in the open hole tension (OHT) simulation of the composite laminate.

CHAPTER 2
CONTINUUM MODELING

2.1 Theoretical background

The Material Point Method (MPM), first developed by Sulsky *et al.* [16], is an extension of the particle-in-cell (PIC) method and is used as an alternative approach to dynamic Finite Element Method to solve problems with large material deformations. MPM is a mixed Lagrangian and Eulerian method, in which particles store all the information of the material at each time step and represents the discrete Lagrangian state of the continuum. The background Eulerian grid is essentially used as a scratch pad, and is reset to its original position after each timestep (See schematic in Fig. 1). Therefore, MPM does not require remeshing and remapping of state variables when dealing with large deformation problems like impact, penetration, fragmentation and fracture. MPM starts with the conservation of linear momentum

$$\nabla \cdot \boldsymbol{\sigma} + \rho \mathbf{b} = \rho \mathbf{a} \quad (2)$$

where $\boldsymbol{\sigma}$ is the stress tensor, \mathbf{b} is the body force vector, \mathbf{a} is the acceleration vector and ρ is the density.

The weak form of Eq. (2) can be obtained as

$$\int_{\Omega} \rho \mathbf{a} \cdot \delta \mathbf{v} dV + \int_{\Omega} \rho \boldsymbol{\sigma}^s \cdot \nabla \delta \mathbf{v} dV = \int_{\Omega} \rho \mathbf{b} \cdot \delta \mathbf{v} dV + \int_{\partial \Omega} \rho \boldsymbol{\tau}^s \cdot \delta \mathbf{v} dS \quad (3)$$

where specific stress is $\sigma_{ij}^s = \sigma_{ij} / \rho$, specific traction is $\tau_i^s = \tau_i / \rho$, $\delta \mathbf{v}$ is the admissible velocity vector, and Ω is the material domain. In the MPM method, density can be expressed as

$$\rho(\mathbf{x}) = \sum_{p=1}^{n_p} m_p \Delta(\mathbf{x} - \mathbf{x}_p) \quad (4)$$

where p stands for the p^{th} particle, m_p is the mass of the p^{th} particle, n_p is the total number of the particles, \mathbf{x}_p is the position vector of the p^{th} particle and Δ is the Dirac delta function.

Substituting Eq. (4) into Eq. (3), we get

$$\sum_{p=1}^{n_p} m_p \mathbf{a}_p \cdot \delta \mathbf{v}_p + \sum_{p=1}^{n_p} m_p \boldsymbol{\sigma}_p^s \cdot \delta \mathbf{v}_p = \sum_{p=1}^{n_p} m_p \mathbf{b}_p \cdot \delta \mathbf{v}_p + \sum_{p=1}^{n_p} m_p \boldsymbol{\tau}_p^s h^{-1} \cdot \delta \mathbf{v}_p \quad (5)$$

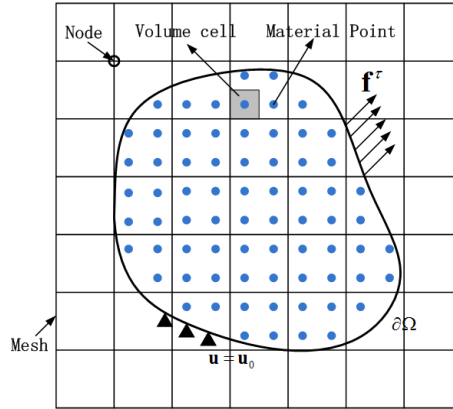


Figure 2.1 Lagrangian Material points distributed on a background Eulerian grid

where h is the thickness of the boundary. Each property of the particle can be interpolated from the nodal information by making use of the shape function.

$$\phi_p = \sum_{p=1}^{n_p} N_I(\mathbf{x}_p) \phi_I \quad (6)$$

$$\nabla \phi_p = \sum_{p=1}^{n_p} \nabla N_I(\mathbf{x}_p) \phi_I \quad (7)$$

$$\delta \phi_p = \sum_{p=1}^{n_p} N_I(\mathbf{x}_p) \delta \phi_I \quad (8)$$

where ϕ_p is the particle property, ϕ_I is the nodal property and $N_I(\mathbf{x})$ is the interpolation function for node I . Substituting Eqs. (6), (7), (8) into Eq. (5) leads to

$$\dot{\mathbf{p}}_I = \mathbf{f}_I^{\text{int}} + \mathbf{f}_I^{\text{ext}} \quad (9)$$

where

$$\mathbf{p}_I = \sum_J^{n_g} m_{IJ} \mathbf{v}_J \quad (10)$$

$$\mathbf{f}_I^{\text{int}} = - \sum_{p=1}^{n_p} V_p \boldsymbol{\sigma}_p \nabla N_I(\mathbf{x}_p) \quad (11)$$

$$\mathbf{f}_I^{\text{ext}} = \sum_{p=1}^{n_p} m_p N_I(\mathbf{x}_p) \mathbf{b}_p + \sum_{p=1}^{n_p} V_p N_I(\mathbf{x}_p) \boldsymbol{\tau}_p h^{-1} \quad (12)$$

$$m_{IJ} = \sum_{p=1}^{n_p} m_p N_I(\mathbf{x}_p) N_J(\mathbf{x}_p) \quad (13)$$

where n_g is the number of the nodes and the number of active grid nodes can be applied in order to reduce computation costs. Lumped mass matrix is usually applied in Eq. (10) to simplify calculations in MPM. Hence, the nodal mass is given by

$$m_I = \sum_{p=1}^{n_p} m_p N_I(\mathbf{x}_p) \quad (14)$$

Various time integration algorithms can be implemented to solve Eq.(9), which is the momentum equation on grid nodes. The Euler forward time discretization scheme is applied in this work to accomplish time integration explicitly.

GIMP, developed by S.G.Bardenhagen and E.M.Kober [17], stands for Generalized Interpolation Material Point and it is a generalized version of MPM. The GIMP shape function

and its gradient can be given by

$$\bar{S}_{ip} = \frac{\int_{\Omega_p} \chi_p(\mathbf{x}) N_i(\mathbf{x}) dV}{\int_{\Omega_p} \chi_p(\mathbf{x}) dV} \quad (15)$$

$$\bar{\nabla S}_{ip} = \frac{\int_{\Omega_p} \chi_p(\mathbf{x}) \nabla N_i(\mathbf{x}) dV}{\int_{\Omega_p} \chi_p(\mathbf{x}) dV} \quad (16)$$

where $\chi_p(\mathbf{x})$ is the particle shape function or particle characteristic function and Ω_p is the domain of the particle. When $\chi_p(\mathbf{x})=1$ at Ω_p , the method becomes the GIMP approach presented by S.G.Bardenhagen and E.M.Kober [17]; when $\chi_p(\mathbf{x}) = \delta(\mathbf{x})$, the method recovers to the classic MPM as was described in the beginning.

GIMP solves the cell crossing issue of MPM which comes from the shape function. However, in practice, we find that GIMP does not perform well when doing mesh refinement using a fixed refined mesh. To overcome this problem, adaptive mesh refinement needs to be applied. Tan and Nairn [51] and Ma *et al.* [52] reported the first implementation of the Structured Adaptive Mesh Refinement Application Infrastructure (SAMRAI). It is also found that the classic MPM alone can perform well in mesh refinement without adaptive refinement by involving the five-node element and we will discuss this topic in section 2.3.

2.2 Explicit time integration

The Modified Update Stress Last (MUSL) scheme, which is proposed by Sulsky *et al.* [16], is adopted in our explicit time integration procedure of the MPM, in order to avoid the numerical problem caused by the small mass of the material point.

From Eq. (11) and (12), the total nodal force can be obtained as

$$\mathbf{f}_I^{\text{tot},t} = \mathbf{f}_I^{\text{int},t} + \mathbf{f}_I^{\text{ext},t} \quad (17)$$

The momenta for the next time step will then be updated as

$$\mathbf{p}_I^{t+\Delta t} = \mathbf{p}_I^t + \Delta t \mathbf{f}_I^{tot,t+\Delta t} \quad (18)$$

The particle velocities and positions will then be mapped from the nodes

$$\mathbf{v}_p^{t+\Delta t} = \mathbf{v}_p^t + \Delta t \sum_{I=1}^{n_g} N_I(\mathbf{x}_p^t) \frac{\mathbf{f}_I^t}{m_I^t} \quad (19)$$

$$\mathbf{x}_p^{t+\Delta t} = \mathbf{x}_p^t + \Delta t \sum_{I=1}^{n_g} N_I(\mathbf{x}_p^t) \frac{\mathbf{p}_I^{t+\Delta t}}{m_I^t} \quad (20)$$

In MUSL, the nodal velocity will then be updated as

$$\mathbf{v}_I^{t+\Delta t} = \sum_{p=1}^{n_p} N_I(\mathbf{x}_p) \frac{\mathbf{p}_p^{t+\Delta t}}{m_I^t} \quad (21)$$

The gradient of the velocity can be found as

$$\mathbf{L}_p^{t+\Delta t} = \sum_{I=1}^{n_g} \nabla N_I(\mathbf{x}_p) \mathbf{v}_I^{t+\Delta t} \quad (22)$$

According to the deformation gradient and the velocity gradient relation:

$$\dot{\mathbf{F}} = \mathbf{L}\mathbf{F} \quad (23)$$

The deformation gradient tensor can be determined by

$$\mathbf{F}_p^{t+\Delta t} = (\mathbf{I} + \mathbf{L}_p^{t+\Delta t} \Delta t) \mathbf{F}_p^t \quad (24)$$

The strain will be updated using the deformation gradient, as

$$\boldsymbol{\varepsilon}_p^{t+\Delta t} = \frac{1}{2} \left[(\mathbf{F}_p^{t+\Delta t})^T + \mathbf{F}_p^{t+\Delta t} \right] - \mathbf{I} \quad (25)$$

For isotropic linear elastic material, according to material constitutive relations, the stress can be written as

$$\boldsymbol{\sigma}_p^{t+\Delta t} = \lambda \text{tr}(\boldsymbol{\varepsilon}_p^{t+\Delta t}) \mathbf{I} + 2\mu \boldsymbol{\varepsilon}_p^{t+\Delta t} \quad (26)$$

where λ is the Lamé modulus and μ is the shear modulus, which can be written in terms of Young's modulus E and Poisson's ratio ν as

$$\lambda = \frac{E\nu}{(1+\nu)(1-2\nu)} \quad (27)$$

$$\mu = \frac{E}{2(1+\nu)} \quad (28)$$

The convected particle MPM is considered here, so that, the particle domain will be changing through time. Thus, the particle volume is updated according to the following equation.

$$V_p^{t+\Delta t} = \det \mathbf{F}_p^{t+\Delta t} V_p^0 \quad (29)$$

From Eq.(29), the density of the particle can also be updated using the following equation.

$$\rho_p^{t+\Delta t} = \frac{\rho_p^t}{\det \mathbf{F}_p^{t+\Delta t}} \quad (30)$$

After the above procedures, the grid is reset to the original state and the simulation will advance to the next time step.

MUSL formulation is the most common way to do integration for MPM. On the other hand, Update Stress First (USF) and Update Stress Average (USAVG), as proposed by Narin [38], can also be adopted in MPM. It has been observed that the USAVG method is analogous to using half the time step without the cost of doubling the number of calculations and is also showed better energy conservation.

In explicit MPM computations, the Courant-Friedrichs-Lewy condition (CFL condition) is required to ensure the convergence of the calculation. According to CFL, the time step, Δt , must satisfy:

$$\Delta t \leq \frac{\Delta x}{v} \quad (31)$$

where Δx is the minimum dimension of the cell in the background grid and v is the maximum wave speed in the material.

2.3 Mesh refinement

To build a large concurrently coupled model to simulate, for example, crack propagation in a compact tension test, mesh refinement is required. For 2D problems, the regular 4-node isoparametric rectangular element is usually used and the standard shape function can be written as

$$\hat{N}_I(\xi, \eta) = \frac{1}{4}(1 + \xi\xi_I)(1 + \eta\eta_I) \quad I = 1, 2, \dots, 4 \quad (32)$$

where $\xi \in [-1, 1]$, $\eta \in [-1, 1]$ are the natural coordinates, ξ_I, η_I are nodal natural coordinates of the element which take the value of -1 and +1. For the proper transitioning from the MPM material points to an atomistic (MD) model, some mesh refinement may become necessary. The shape function for the 5-node quadrilateral element (shown in Figure 2.2) is able to connect grid of different sizes, as shown in Figure 2.3, and its shape function can be constructed as

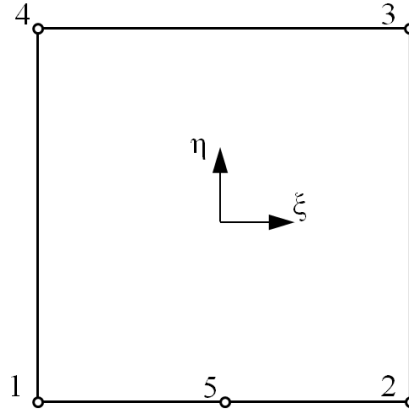


Figure 2.2 Five-node linear element

$$N_1(\xi, \eta) = \hat{N}_1(\xi, \eta) - \frac{1}{2}N_5(\xi, \eta) \quad (33)$$

$$N_2(\xi, \eta) = \hat{N}_2(\xi, \eta) - \frac{1}{2}N_5(\xi, \eta) \quad (34)$$

$$N_3(\xi, \eta) = \hat{N}_4(\xi, \eta) \quad (35)$$

$$N_4(\xi, \eta) = \hat{N}_4(\xi, \eta) \quad (36)$$

$$N_5(\xi, \eta) = \frac{1}{2}(1 - |\xi|)(1 - \eta) \quad (37)$$

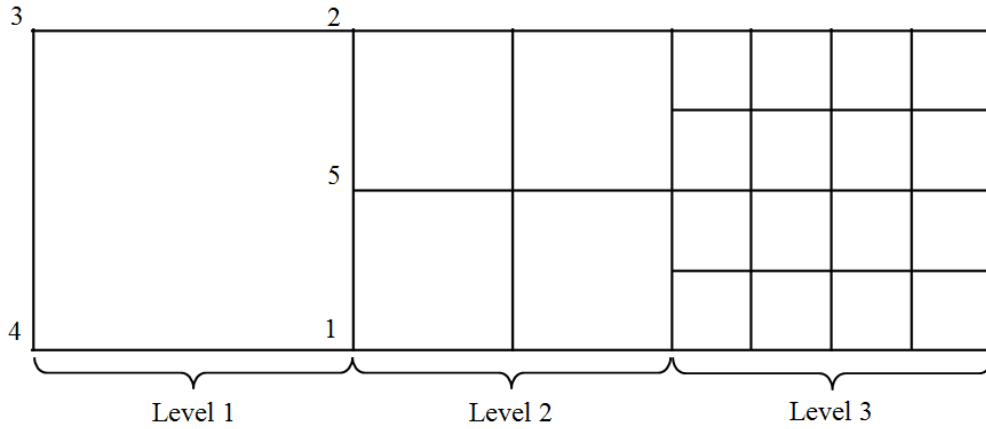


Figure 2.3 Three level of refined meshes from transitioning

2.4 Crack modeling in MPM

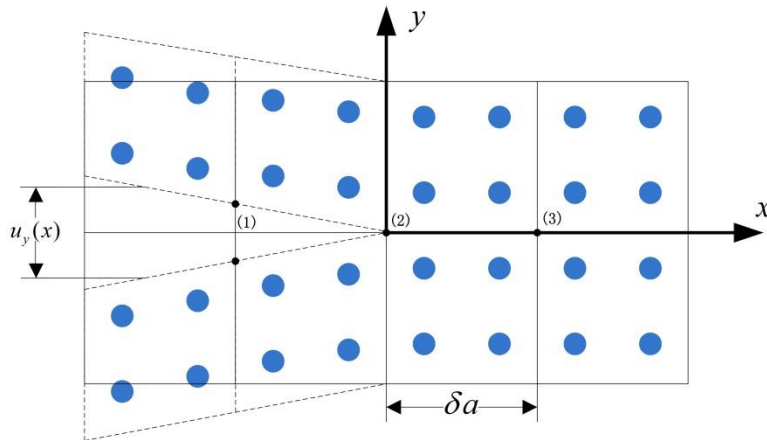


Figure 2.4 Schematic for determining strain energy release rate (SERR) in GIMP

CRAMP, which stands for “CRACKs” with “Material Points”, is the algorithm developed by Nairn [4] to model explicit cracks in MPM scheme. CRAMP allows multiple velocity fields at

special nodes close to cracks, so that conventional MPM which enforces velocity and displacement continuity though grid meshes is extended to be compatible with displacement and velocity discontinuities of certain degree. Three types of velocity fields are defined on the nodes near cracks by using line-crossing algorithm:

$$v(p,i) = \begin{cases} 0 & \text{if line does not cross any crack} \\ 1 & \text{if line crosses a crack from above} \\ 2 & \text{if line crosses a crack from below} \end{cases} \quad (38)$$

where, $v(p,i)$ is the value defining the relative position of the material points, nodes and the crack by drawing a line from particle p to node i . In this way, nodal momenta and lumped masses near the crack can be extrapolated from the corresponding material points using $v(p,i)$.

Once the velocity fields are determined, the modified MPM extrapolations become

$$\left. \begin{aligned} \mathbf{p}_{i,j}^k &= \sum_{p=1}^{n_p} m_p \mathbf{v}_p^k S_{i,p}^k \delta_{j,v(p,i)} \\ m_{i,j}^{Dk} &= \sum_{p=1}^{n_p} m_p S_{i,p}^k \delta_{j,v(p,i)} \end{aligned} \right\} j = 0, 1, 2 \quad (39)$$

in which, each node may have one to three velocity fields denoted by index j on nodal momentum $\mathbf{p}_{i,j}^k$, and $m_{i,j}^{Dk}$ is the nodal mass in the lumped (or Diagonal) mass matrix which have one to three velocity fields. The superscript k indicates these terms apply to the k^{th} MPM step. \mathbf{v}_p^k is particle velocity, m_p is particle mass, $S_{i,p}^k$ is the shape function for node i evaluated at the current position of particle p . $\delta_{j,v(p,i)}$ is the Kronecker delta function.

In this dissertation, dynamic strain energy release rates (SERR) is calculated using virtual crack closure technique (VCCT) [19] and the dynamic (i.e., with inertial effects included) version of the J-integral [20] (Guo & Nairn, 2004).

Figure 2.4 is a schematic of mode I crack in GIMP. For a traction free crack, the crack closure integral in mode I and mode II are given by,

$$G_I = \lim_{\delta a \rightarrow 0} \frac{1}{2\delta a} \int_0^{\delta a} \sigma_{yy}(x) \Delta u_y(x - \delta a) dx \quad (40)$$

$$G_{II} = \lim_{\delta a \rightarrow 0} \frac{1}{2\delta a} \int_0^{\delta a} \tau_{xy}(x) \Delta u_x(x - \delta a) dx \quad (41)$$

Writing the stresses as a linear interpolation between nodal values at nodes (2) and (3) in Fig. 4, and the displacements as linear interpolations between nodes (1) or (1') and (2),

$$\sigma_{yy}(x) = \sigma_{yy}^{(2)} \left(1 - \frac{x}{\delta a}\right) + \sigma_{yy}^{(3)} \frac{x}{\delta a} \quad (42)$$

$$\Delta u_y(x) = \Delta u_y^1 \left(1 - \frac{x}{\delta a}\right) + \Delta u_y^0 \frac{x}{\delta a} = \Delta u_y^1 \left(1 - \frac{x}{\delta a}\right) \quad (43)$$

Substituting Equation (42) into the crack closure integral (Equation (40)) leads to,

$$G_I = \frac{u_y^{(1)} - u_y^{(1')}}{12} (2\sigma_{yy}^{(2)} + \sigma_{yy}^{(3)}) \quad (44)$$

For the polymer being modelled, the critical energy release rate G_{IC} is a known material property. In the proposed GIMP approach, it is assumed that when G_I is greater than G_{IC} ($G_I \geq G_{IC}$), the crack initiates and propagates through separation of the grid nodes at the crack tip.

2.5 Verification of MPM dynamics

In order to couple the MPM code with MD, explicit MPM is adopted in our coupling scheme, because the MD is a dynamical method which is based on Newton's equation of motion. In this manner, the two approaches can be incorporated with each other instinctively. However, the dynamical behavior in the explicit MPM is driven by the position evolution of the material points through time, which can be achieved by applying various time integration algorithms, such as Verlet Integration. It has also been found from our simulation experiences that certain parameters have effect on the dynamical behavior of the model in MPM simulations. To keep the material realistic, the parameters related to the properties of the material, such as density and Young's modulus, need to be kept as real material, which can be obtained from MD simulations. One parameter has relatively large influence to the MPM behavior is the damping term. The damping parameter is applied as a damping of the time integration of the momentum equation on grid nodes, which can be presented as

$$\mathbf{p}_I^{t+\Delta t} = \mathbf{p}_I^t + (1-c)\Delta t \mathbf{f}_I^{\text{tot},t+\Delta t} \quad (45)$$

where c is the damping term.

The MPM results are compared with the solution of vibration of continuous system. The following case (as shown in Figure 2.5) is studied:

A single harmonic force $P(t) = P_0 \sin(\omega t)$ is applied at $x = a$ of a simply-supported bar. The initial condition is

$$w(x, 0) = 0 \quad (46)$$

$$\frac{\partial w}{\partial t}(x, 0) = 0 \quad (47)$$

where $0 \leq x \leq L$, $w(x,t)$ represent the deflection of the beam.

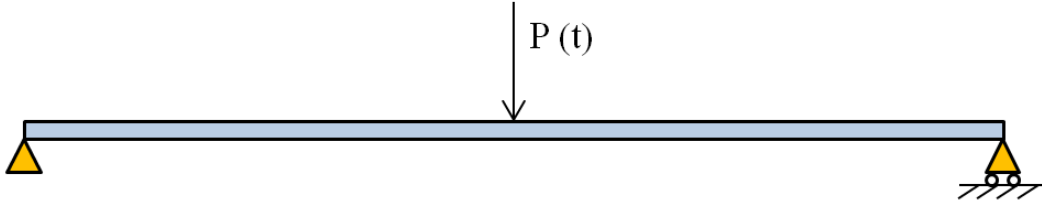


Figure 2.5 MPM dynamics test case: A simply-supported bar with a single harmonic force

The equation governing beam's deflection can be written as

$$\frac{d^2}{dx^2} \left[EI(x) \frac{d^2 w(x)}{dx^2} \right] = p(x) \quad (48)$$

where $EI(x)$ is the bending stiffness, $p(x)$ is the distributed transverse load. By solving Eq. (48), we get

$$w(x,t) = \frac{2P_0L^3}{\pi^4 EI} \left[\sum_{n=1}^{\infty} \frac{\sin\left(\frac{n\pi a}{L}\right) \sin\left(\frac{n\pi x}{L}\right)}{n^4 - \left(\frac{\omega}{\omega_1}\right)^2} \right] \sin(\omega t) - \frac{2\frac{\omega}{\omega_1} P_0L^3}{\pi^4 EI} \left[\sum_{n=1}^{\infty} \frac{\sin\left(\frac{n\pi a}{L}\right) \sin\left(\frac{n\pi x}{L}\right)}{n^2 \left[n^4 - \left(\frac{\omega}{\omega_1}\right)^2 \right]} \right] \sin(n^2 \omega_1 t) \quad (49)$$

where $\omega_1 = \frac{\pi^2}{L^2} \sqrt{\frac{EI}{\rho A}}$ is the fundamental characteristic frequency of the bar.

To compare the MPM dynamical behavior with the exact solution we got, a case of beam deflection with a harmonic force applied in the middle with frequency $\omega = \pi/2$ is studied. The exact solution and the MPM results for different damping value are compared as shown in Figure 2.6. Damping can go from 0 (no damping) to 1 (full damping). With zero damping, the deflection changes a little faster than the exact solution; while with high damping value (more than 0.5), the system to start to deviate from the exact solution and shows time lag comparing with the solution. It is found that 0.25 is an acceptable value to capture the shape of the exact solution with maximum error equals 0.71%. Therefore, the damping term is set to be 0.25 in MPM simulation to ensure the correct dynamical behavior of the continuum model.

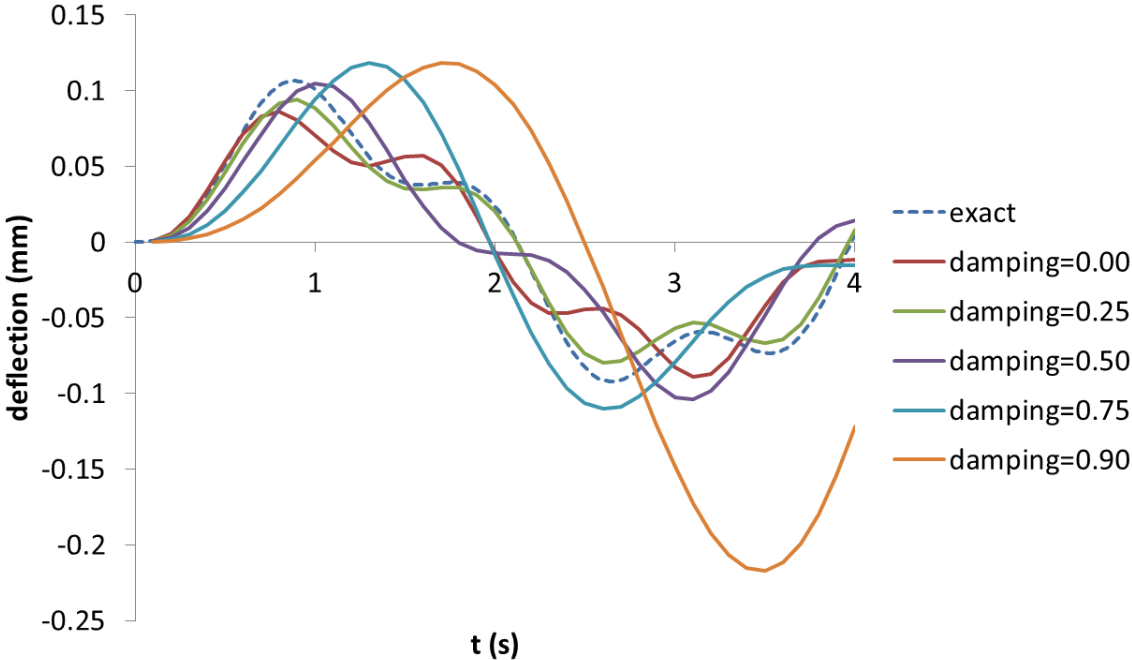


Figure 2.6 Case study: beam deflection vs. time

2.6 Stress wave propagation in MPM

Unlike the static or semi-static method, MPM does not instantly get the final state of the system under certain boundary conditions, on the opposite, it takes certain amount of time for the effect of boundary condition to propagate through the whole body by means of propagation of information through material points and grid nodes. As shown in Figure 2.7, the properties like velocities and positions of the local material are restored at the corresponding material points at current time step t ; the information is transferred to the grid nodes by extrapolation through particle shape function at the next time step $t + \Delta t$; after the momentum equation is solved on the grid nodes for time $t + \Delta t$, the information will be interpolated back and restored on the material points. The grid node is going to be reset at the end of time $t + \Delta t$ while the material points are updated from the new information. In this way, the grid information is updated through the simulation by means of restoring the information on material points at each time step. Therefore, stress wave can be propagated through the MPM model in this manner.

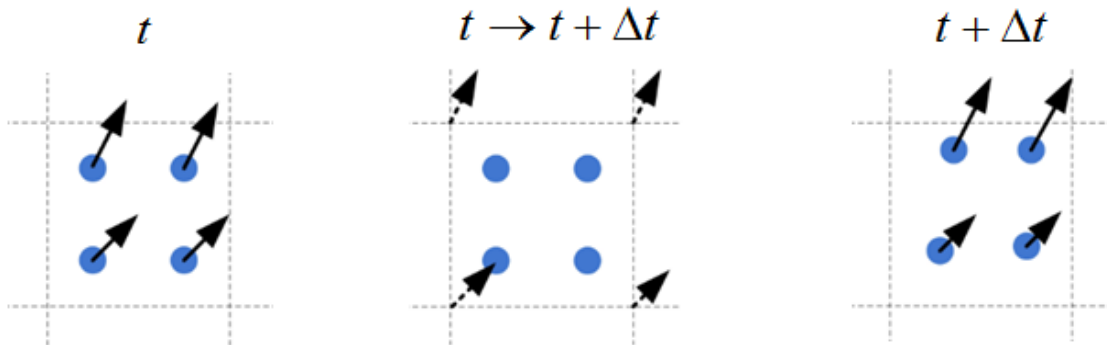


Figure 2.7 Information updating of material points and grid nodes

However, the wave propagation is a nature of the explicit time integration scheme of MPM and the process need to be verified. A bar with the length of 100 meters under a constant load (100MPa) is studied to accomplish this goal.



Figure 2.8 Wave propagation on a bar

From the material properties, the wave speed for one-dimensional solids can be estimated as

$$v_c = \sqrt{\frac{E}{\rho}} \quad (50)$$

Using the Young's modulus and density of graphene, we can get $v_c = 21.4km/s$.

By rescaling the time step for MPM simulations, the results of wave propagation can be obtained as shown in Figure 2.9. The external influence propagates through the length of the bar within 0.05ms. From the figure, it can be seen that, as the wave pass through, the stress rises to about 120MPa first then damps quickly until reaching 100MPa, due to the characteristic of material points. By rescaling the time step value, a wave speed of 20.0km/s can be achieved by this model. Comparing with the real value of v_c obtained from Eq.(50), this value is close enough to simulate the real material and to couple with molecular dynamics model to simulate the real material.

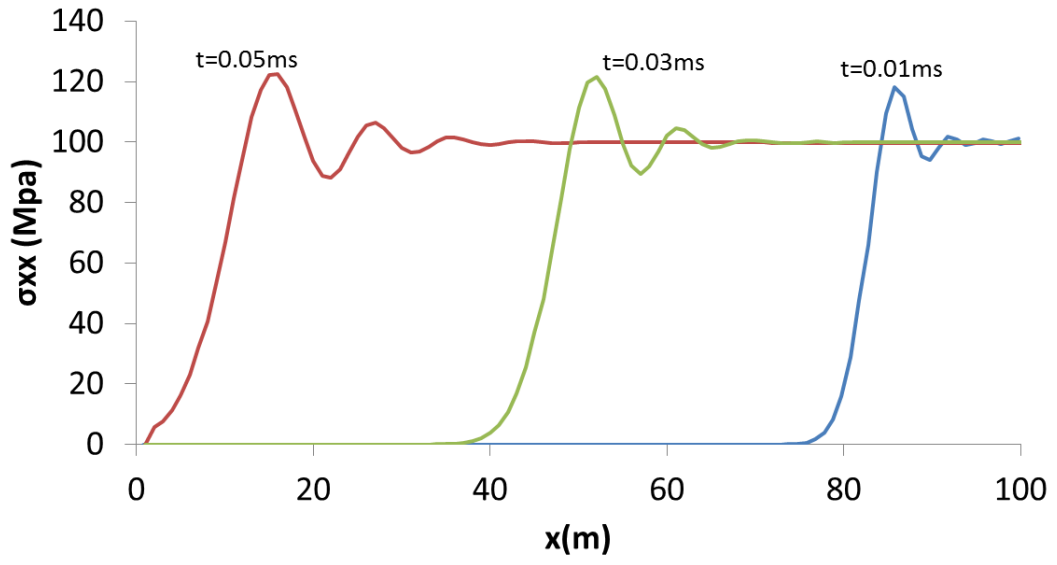


Figure 2.9 Wave propagation of the MPM simulation

CHAPTER 3

MOLECULAR DYNAMICS

3.1 Introduction

Molecular Dynamics (MD) is a simulation technique based on Newtonian mechanics for studying the movements of the atoms and molecules as well as the interactions between the particles. The method was introduced independently by Fermi, Pasta, and Ulam [39], Alder and Wainwright [40] and Rahman [41]. Since 1970s, applications of MD became frequent in modeling three-dimensional structures of proteins and other macromolecules. MD is used to study the dynamics of the phenomena at atomic level which cannot be examined directly and also became useful to help scientists interpret biophysical experimental results. Progress of MD in prediction of experiments relies on the improvements in computational resources and the quality of force field parameters. MD approach limited itself in not only the parameter sets applied in the simulation, but also in the adopted force fields. Generally, MD is unable to make accurate predictions of long term responses of the atomistic system due to errors from the force field parameter sets.

From multiscale aspect, MD simulations can also be viewed as a bridge between the deterministic behavior of the macroscopic material system and the statistical nature of atomistic interactions. MD offers us possibility to predict the time evolution of a system of interacting particles and estimate the relevant physical properties. Nowadays, MD is used very frequently in analyzing small-scale behavior of material for the reason that it is able to capture complex interactions of particles at molecular level and help us to better understand the nano-scale

phenomena in a theoretical framework. Thermodynamic and mechanical properties can even be estimated statistically using MD if a sufficient number of atoms are included in the molecular model.

For an N-atom molecular system, from Newton's law, we have the classical equations of motion of atom i as,

$$m_i \frac{d^2 \mathbf{x}_i^t}{dt^2} = -\nabla_i V(\mathbf{x}_1^t, \mathbf{x}_2^t, \dots, \mathbf{x}_N^t) \equiv \mathbf{F}_i^t \quad (i = 1, 2, \dots, N) \quad (51)$$

where, m_i , \mathbf{x}_i^t is mass and position of atom, respectively. The internal force \mathbf{F}_i of atom i is computed from the prescribed energy potential V which describes the interaction of atom i with all other atoms in the molecular system. Hence, MD models are inherently nonlocal.

Deformations, if any, are applied to the system of atoms. Temperature and pressure are maintained using appropriate thermostat and barostat respectively. Using the formula given by equation (51), forces on each atom (\mathbf{F}_i^t) at any time are calculated as derivatives of the potential function. The interaction energy and forces are computed by summing each pairwise interaction of an atom with its neighbors.

3.2 Numerical integration

Various numerical integration schemes are then used to determine the updated positions of each atom for the next time step. This process is repeated until the termination condition is reached, which is usually the specified number of timesteps.

Verlet integration algorithm, which is commonly used to calculate the trajectories of particles in MD simulations, is implemented as the numerical integration method in this dissertation. It is frequently applied to calculate trajectories of particles in molecular dynamics simulations and

computer graphics, for the reason that it provides good numerical stability and has the good features like time-reversibility and preservation of the symplectic form on phase space with no significant additional computational cost comparing to Euler method.

The basic form of Verlet algorithm does not generate velocities directly and the error calculated from the positions is of order two rather than four. A better version of the same basic algorithm, Velocity Verlet integration algorithm, solves this problem. In Velocity Verlet, velocity v and positions r at time $t + \Delta t$ are given by,

$$v(t + \Delta t) = v(t) + \frac{1}{2}(a(t) + a(t + \Delta t))\Delta t \quad (52)$$

$$r(t + \Delta t) = r(t) + v(t)\Delta t + \frac{1}{2}a(t)\Delta t^2 \quad (53)$$

Using the equations above, the approach updates atom positions and velocities without compromising on the precision, which was encountered in the original Verlet algorithm. The global error of Velocity Verlet is of order two.

3.3 Potential function

In MD simulations, it is vital for the potential function to be appropriately defined due to the fact that it determines the movements of the atoms or particles. Traditionally, in non-reactive MD, interactions between atoms are modeled with fixed-topology force fields where bonds are defined before the MD simulation starts and atoms remain bonded throughout the simulation.

The Optimized Potential for Liquid Simulations (OPLS) force field, developed by Jorgensen WL [42], is a traditional potential function which is widely adopted for MD simulation of polymers. The OPLS force field can be represented as the sum of the energy from bonded and non-bonded interactions. The part of the bonded interactions can be divided into interactions

from the bonds, angles and dihedrals. Thus, the functional form of OPLS force field can be written as

$$E_{system} = E_{bonds} + E_{angles} + E_{dihedrals} + E_{nonbonded} \quad (54)$$

In Eq.(54), the term for the interaction of bonds and angles can be written as harmonic form. The Lennard-Jones force field, which has strongly repulsive core and weakly attractive tail, is used to imitate the van der Waals interaction and used as the nonbonded term. Lennard-Jones 6-12 potential can be expressed as

$$V_{LJ}(r_{ij}) = 4\varepsilon_{ij} \left[\left(\frac{\sigma_{ij}}{r_{ij}} \right)^{12} - \left(\frac{\sigma_{ij}}{r_{ij}} \right)^6 \right] \quad (55)$$

where r_{ij} is the distance between the two non-bonded atoms, i and j , the well depth parameter ε is considered to be the geometric mean of the values of the respective atom types, and the equilibrium spacing parameter σ determines the arithmetic mean of the individual parameters of the respective atom types.

However, in order to simulate fracture behavior of the material, such as crack initiation and propagation during the fracture process, bond formation and breakage is required in the simulation. ReaxFF, which stands for Reactive Force Field and was developed by van Duin *et al.* [31], provides us a way to simulate continuous bond formation and breaking. In ReaxFF, a bond-order potential based reactive force field is defined and it can accurately simulate bond formation and breaking within every iterative time step. A number of parameters which can be derived from quantum chemical theories on bond dissociations and reactions of molecules are required in ReaxFF simulations. Differently from OPLS, the system energy can be written as,

$$\begin{aligned}
E_{system} = & E_{bond} + E_{lp} + E_{over} + E_{under} + E_{val} + E_{pen} + E_{coa} + E_{vdWaals} \\
& + E_{C2} + E_{tors} + E_{conj} + E_{H-bond} + E_{vdWaals} + E_{Coulomb}
\end{aligned}
\tag{56}$$

Each partial energy term in the above equation is a function of bond order, which can be formulated using interatomic distance. The general form of bond order BO_{ij} between two atoms i and j can be written as,

$$BO_{ij} = \exp \left[p_{bo,1} \cdot \left(\frac{r_{ij}}{r_0} \right)^{p_{bo,2}} \right]
\tag{57}$$

where r_{ij} is the current distance between atoms i and j , r_0 is the equilibrium distance, $p_{bo,1}$ and $p_{bo,2}$ are bond parameters (constants). Bond separation is assumed to occur when the bond order between a pair of atoms goes to zero. Given the bond order, the bond energies can be estimated by

$$E_{bond} = -D_e \cdot BO_{ij} \cdot \exp \left[p_{be,1} \left(1 - BO_{ij}^{p_{be,1}} \right) \right]
\tag{58}$$

where D_e and $p_{be,1}$ are the bond parameters.

The other terms in Eq.(56) can be found in [31] and they have similar forms which can be written as a function of bond order. From Eq.(57) and (58), it can be observed that the bond energies only depend on the interatomic distance. Therefore, dynamic formation and breakage of the chemical bonds can be simulated by keeping track of the bond order. ReaxFF is used in the MPM/MD coupling simulation, because one of the main purposes of this research is to study the fracture behavior of polymers.

3.4 Ensembles

An ensemble is defined as a collection of all possible systems which have different microscopic states but have an identical macroscopic or thermodynamic state. In molecular dynamics simulations, the temperature and pressure of the system may be kept constant to mimic the realistic experimental conditions. For a N -atom MD system, the ensemble average is given by

$$\langle A \rangle_{ensemble} = \iint A(p^N, r^N) \rho(p^N, r^N) dp^N dr^N \quad (59)$$

where $A(p^N, r^N)$ is the observable of interest and it can be written as a function of the momenta p , and the position r of the systems. The probability density is expressed as

$$A(p^N, r^N) = \frac{1}{Q} \exp \left[\frac{-H(p^N, r^N)}{k_B T} \right] \quad (60)$$

where H is the Hamiltonian, T is the temperature, k_B is Boltzmann's constant and Q is the partition function

$$Q = \iint \exp \left[\frac{-H(p^N, r^N)}{k_B T} \right] dp^N dr^N \quad (61)$$

Due to the difficulty to estimate Eq.(61), another way is used to determine a time average of A in MD simulations, which is given by

$$\langle A \rangle_{time} = \lim_{\tau \rightarrow \infty} \frac{1}{\tau} \int_{t=0}^{\tau} A(p^N(t), r^N(t)) dt \approx \frac{1}{M} \sum_{t=1}^M A(p^N, r^N) \quad (62)$$

where τ is the simulation time, M is the number of time steps in the MD simulation and $A(p^N(t), r^N(t))$ is the instantaneous value of A at time t .

It should be noticed that the Ergodic hypothesis needs to be adopted in here, which states that

$$\langle A \rangle_{ensemble} = \langle A \rangle_{time} \quad (63)$$

Ergodic hypothesis allows the system to evolve in time so that the system will eventually pass through all possible states. Different statistical ensembles could be applied depending on which state parameters are kept fixed. The state variables usually include the energy E , temperature T , pressure P , volume V , and number of particles N . The following three types of ensembles are the most commonly used ones in MD simulations.

1. NVE Ensemble

The constant-energy, constant-volume ensemble (NVE), also known as the microcanonical ensemble, is obtained by solving Newton's equation of motion without any temperature and pressure control. In NVE, energy is conserved and is usually used for a process where the system is isolated. However, due to rounding and truncation errors of the numerical integration process, a slight drift in energy is always observed. NVE ensemble is not recommended for equilibration because of the difficulty in keeping the system at the desired temperature range. In practice, it is observed that NVE ensemble has better performance in wave propagation simulations, however, the temperature is always difficult to control and may go too high for certain simulations.

2. NVT Ensemble

The constant-temperature, constant-volume ensemble (NVT) is known as the canonical ensemble. The temperature is controlled by direct temperature scaling during the initialization phase and temperature-bath coupling during the data collection period. This ensemble is suitable for the system with a heat bath at the assigned temperature. Many types of thermostat algorithms can be adopted to add or remove energy from the boundaries in a realistic way. Different thermostats include Nose-Hoover, Berendsen, Andersen etc. can be used in NVT.

3. NPT Ensemble

The constant-temperature, constant-pressure ensemble (NPT) controls both the temperature and pressure of the system. The pressure is adjusted by changing the volume in NPT. If the correct pressure, volume, and densities are important for the system, NPT ensemble is the good choice. This ensemble can also be used during the equilibration in order to reach the desired pressure and temperature before changing to other ensembles.

In molecular dynamics, the required force field is selected to describe the material being studied when the system is initialized. The atomic interaction behavior is completely defined by the choice of different interaction potentials. The molecular system will be allowed to evolve under imposed pressure and temperature state. Periodic boundary conditions (PBCs) are often chosen in MD simulations to calculate bulk materials as it can approximate an infinite system using a relatively small system. In this paper, LAMMPS, a molecular dynamics program developed by Sandia National Laboratories, is used as the MD solver. The ReaxFF (Reactive Force Field) potential has been chosen to simulate polymer atomic interactions in this work. The canonical ensemble, NVT ensemble, in which number of particles, volume and temperature are conserved, is used in the molecular simulations. This ensemble represents a system in thermal equilibrium with a heat bath at the prescribed temperature (T). A suitable thermostat is used to add or remove energy from the MD system. Various types of thermostats like Nose-Hoover, Berendsen, and Andersen etc. are available in MD.

3.5 Atomistic J-Integral calculation

3.5.1 Linear elastic fracture mechanics

Linear elastic fracture mechanics (LEFM) provides the basic concepts and background information of fracture. Stress intensity factor (SIF), K , is a parameter, which is able to characterize the stress state near the crack tips for linear elastic materials. Three typical fracture

modes are shown in Figure 3.1. For the edge-cracked plate case (Figure 3.2), the stress intensity factor for mode I can be expressed as

$$K_I = \sigma \sqrt{\pi a} f\left(\frac{a}{w}\right) \quad (64)$$

where σ is the far field tensile stress applied to the plate, a is the crack length, w is the width of the plate and f is the function related to the geometry. For linear elastic material, stress intensity factor for mode I can also be related with the energy release rate by

$$G_I = \frac{K_I^2}{E} \quad (65)$$

The critical value of K is known as the fracture toughness K_c , which can be considered as a material property in which it describes the fracture strength of the material. When K_c is reached crack tends to advance and same thing can be applied for G_c .

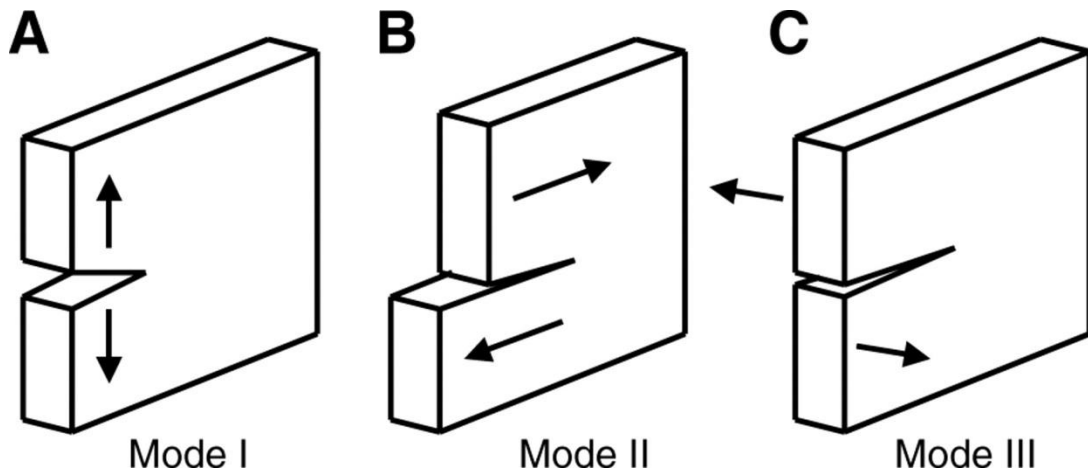


Figure 3.1 Three modes of fracture: (A) mode I: tensile opening; (B) mode II: in-plane shearing; and (C) mode III: out-of-plane shearing

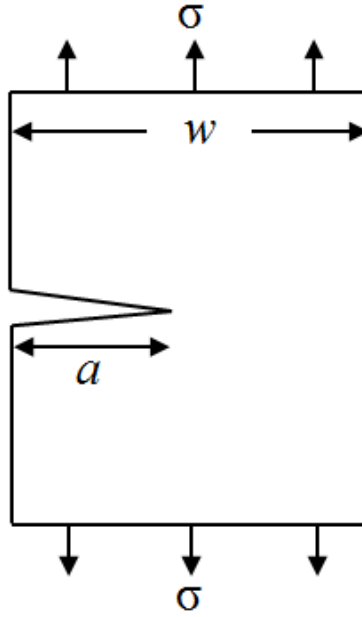


Figure 3.2 Edge-cracked plate under uniform tension loading

3.5.2 J-integral

However, LEFM is proved invalid when significant plastic deformation occurs in fracture. Unlike linear elastic fracture mechanics, the integral provides a way to calculate the strain energy release rate even when nonlinearities, such as crack bridging, are present near the crack tip. J-integral is proposed by J. Rice [43] and can be derived from Eshelby momentum tensor [44].

$$P_{kj} = W \delta_{kj} - \sigma_{ij} \frac{\partial u_i}{\partial x_k} \quad (66)$$

where W is the strain energy density, σ_{ij} is the Cauchy stress tensor, u_i is the displacement vector. Thus, the 3-D form J-integral can be defined as

$$\begin{aligned}
J_k &= \lim_{\varepsilon \rightarrow 0} \oint_{\Gamma_\varepsilon} \left[W \delta_{kj} - \sigma_{ij} \frac{\partial u_i}{\partial x_k} \right] n_j d\Gamma \\
&= \oint_{C+\gamma} \left[W \delta_{kj} - \sigma_{ij} \frac{\partial u_i}{\partial x_k} \right] n_j d\Gamma + \iint_{\Omega(C)} \frac{\partial}{\partial x_3} \left(W \delta_{k3} - \sigma_{i3} \frac{\partial u_i}{\partial x_k} \right) dA \\
&\quad (i, j = 1, 2 \quad k = 1, 2, 3)
\end{aligned} \tag{67}$$

in which, $\Gamma_\varepsilon = -C_\varepsilon$, is the contour near the crack tip as shown in Figure 3.3.

From Eq.(67), three component of the J-integral can be derived as

$$J_1 = \oint_C \left[W n_1 - \sigma_{ij} n_j \frac{\partial u_i}{\partial x_1} \right] d\Gamma \tag{68}$$

$$J_2 = \oint_C \left[W n_2 - \sigma_{ij} n_j \frac{\partial u_i}{\partial x_2} \right] d\Gamma + \oint_\gamma W n_2 d\Gamma \tag{69}$$

$$J_3 = -\oint_C \sigma_{ij} n_j \frac{\partial u_i}{\partial x_3} d\Gamma + \iint_{\Omega(C)} \frac{\partial W}{\partial x_3} dA \tag{70}$$

For mixed mode, J-integral of mode $M=I, II$ and III can be defined as

$$J^M = \lim_{\varepsilon \rightarrow 0} \oint_{\Gamma_\varepsilon} \left[W^M n_1 - \sigma_{ij}^M \frac{\partial u_i^M}{\partial x_1} n_j \right] d\Gamma \tag{71}$$

Moreover, it can be derived that

$$\begin{cases} J_1 = J^I + J^{II} + J^{III} \\ J_2 = -2\sqrt{J^I J^{II}} \end{cases} \tag{72}$$

It should be noticed that $J_k (k = 1, 2, 3)$ is the k^{th} component of the 3-D form J-integral while $J^M (M = I, II, III)$ is the J-integral for the mode M fracture. It has also been proved that J_1 is a path dependent integral, which is able to characterize the fracture behavior of the crack tip.

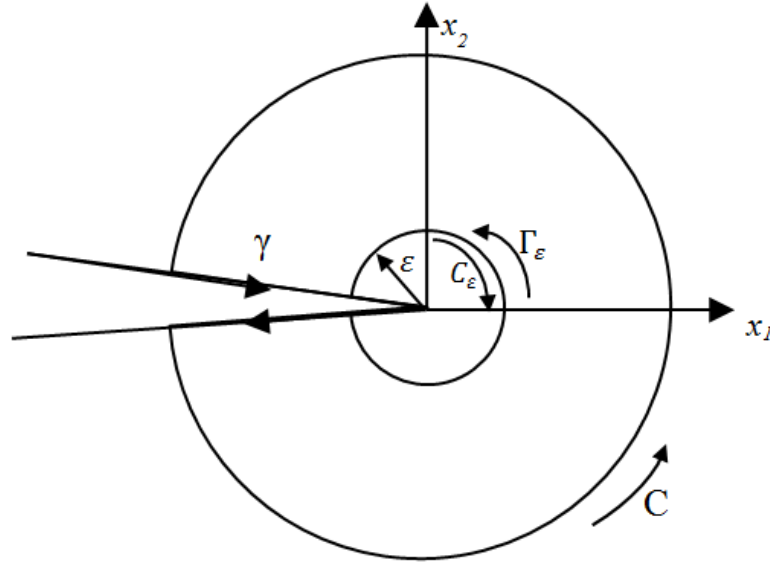


Figure 3.3 Γ_ε and C_ε contour direction

For isotropic, perfectly brittle, linear elastic material, the J-integral is related to the fracture toughness of the material for the typical crack problem. For plane strain problem, the relation can be written as

$$J_c^I = G_{Ic} = K_{Ic}^2 \left(\frac{1-\nu^2}{E} \right) \quad (73)$$

$$J_c^{II} = G_{IIc} = K_{IIc}^2 \left(\frac{1-\nu^2}{E} \right) \quad (74)$$

$$J_c^{III} = G_{IIIc} = K_{IIIc}^2 \left(\frac{1+\nu}{E} \right) \quad (75)$$

J-integral can be considered as an energy-related parameter and, similarly with respect to the usage in linear elastic case, it is able to characterize the intensity of strains near the crack tip in elastic-plastic problems as suggested by Hutchinson [45], Rice and Rosengren [46].

Eq.(68) can also be rewritten as

$$J = \int_C (\Psi \mathbf{N} - \mathbf{H}^T \mathbf{P} \mathbf{N}) dA \quad (76)$$

where $\mathbf{H} = \mathbf{F} - \mathbf{I}$ is the displacement gradient tensor, Ψ is the Helmholtz free energy density and \mathbf{N} is the outward normal vector to the surface C enclosing the region.

3.5.3 Numerical atomistic J estimation

The calculation of J-integral in MD domain can be completed by using Gaussian quadrature integration. A square contour is commonly chosen to do the numerical integration considering the computational efficiency and accuracy. The contour around the crack tip is divided into several line segments as shown in Figure 3.4. In the figure, the yellow points on the integration contour C represent the Gaussian quadrature points. Three Gaussian quadrature points are used on each line segment, so that, from Eq.(68), the integration of each line can be estimated by

$$J_{seg} = \sum_{i=1}^{n_G} w(\mathbf{x}_i) \left(W(\mathbf{x}_i) \mathbf{I} - \nabla_x^T \mathbf{u}(\mathbf{x}_i) \boldsymbol{\sigma}(\mathbf{x}_i) \right) \mathbf{n}_{seg} \quad (77)$$

where w is weight, \mathbf{u} is displacement, $\boldsymbol{\sigma}$ is Cauchy stress and \mathbf{n}_{seg} is the outward normal vector for each segment. In our calculation scheme, n_G is chosen to be 3.

Finite element interpolation functions are used in order to convert the discrete values of potential energy and displacement gradients obtained from MD simulations into the corresponding quantities that can be used in Eq.(77). The nine-node quadratic element is adopted to interpolate the discrete atomistic values on to the Gaussian quadrature points as represented in Figure 3.4. The shape function of the nine-node element can be given by

$$\begin{aligned}
N_1 &= \frac{1}{4} \xi(1-\xi)\eta(1-\eta) \\
N_2 &= -\frac{1}{4} \xi(1+\xi)\eta(1-\eta) \\
N_3 &= \frac{1}{4} \xi(1+\xi)\eta(1+\eta) \\
N_4 &= -\frac{1}{4} \xi(1-\xi)\eta(1+\eta) \\
N_5 &= -\frac{1}{2} (1-\xi)(1+\xi)\eta(1-\eta) \\
N_6 &= \frac{1}{2} \xi(1+\xi)(1-\eta)(1+\eta) \\
N_7 &= \frac{1}{2} (1-\xi)(1+\xi)\eta(1+\eta) \\
N_8 &= -\frac{1}{2} \xi(1-\xi)(1-\eta)\eta \\
N_9 &= (1-\xi^2)(1-\eta^2)
\end{aligned} \tag{78}$$

where ξ and η are local coordinates which go from -1 to 1.

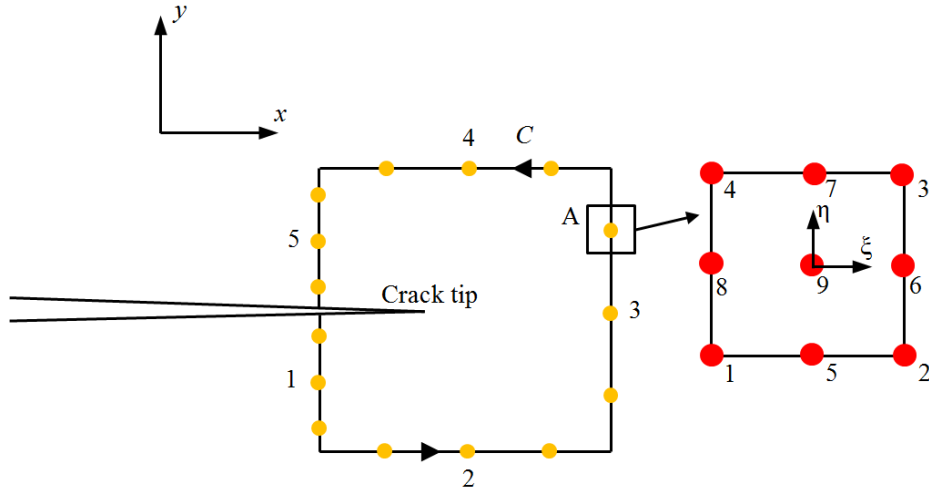


Figure 3.4 J-integral contour and the Gaussian quadrature points

The macroscopic or equivalent continuum stress in molecular scale is commonly evaluated by the virial stress, which was originally found by Irving and Kirkwood [21] and derived by

Cormier *et al.* [22] based on the work of Lutsko [23]. The tensor form of the virial stress can be expressed as

$$\boldsymbol{\sigma}_{virial} = -\frac{1}{\Omega} \sum_{\alpha \in \Omega} \left(\frac{1}{2} \sum_{\beta \neq \alpha} \mathbf{x}^{\alpha\beta} \otimes \mathbf{f}^{\alpha\beta} + m^\beta \mathbf{u}^\alpha \otimes \mathbf{u}^\alpha \right) \quad (79)$$

where, m^β is the mass of the β^{th} molecule in volume Ω , $\mathbf{f}^{\alpha\beta}$ and $\mathbf{x}^{\alpha\beta}$ are the force and position vector between particle α and β , and relative velocity vector is defined as $\mathbf{u}^\alpha \equiv \mathbf{v}^\alpha - \bar{\mathbf{v}}$. By averaging the virial stress, we can get the Cauchy stress needed in Eq.(77).

CHAPTER 4

CONCURRENT MULTISCALE COUPLING SCHEME

4.1 Embedded Statistical coupling method

The embedded statistical coupling method (or ESCM) is developed by Saether *et al.* to couple MD with FEM simulations. The approach is able to solve a coupled boundary value problem (BVP) at the MD/FE interface in a coupling model where MD domain embedded within a finite element domain. In ESCM, volume cells (VC) are constructed at the overlap domain of MD/FEA to communicate information between the internal MD environment and the external continuum (FEA) region. Statistical averaging method over both time and volume in atomistic subdomains at the handshake zone is adopted in this coupling scheme to estimate the nodal displacement boundary conditions for the finite element model.

In ESCM, the MD domain is divided into three sub domains: the surface volume cell (SVC), interface volume cell (IVC) and the inner MD region. Averaged MD displacements at their mass center are computed in the IVCs and apply to the associated interface FE nodes as displacement boundary conditions. In order to increase the computational efficiency and accuracy, a time average over M MD time steps of the averaged mass center displacement, during the MD/FEA coupling simulation.

$$\delta_{IVC,k} = \frac{1}{M} \sum_{i=1}^M (\mathbf{r}_{CM,k}(t_i) - \mathbf{r}_{CM,k}(0)) \quad (80)$$

in which,

$$\mathbf{r}_{CM,k}(t_i) = \frac{1}{n_k} \sum_{j=1}^{n_k} \mathbf{r}_j(t_i) \quad (81)$$

where $\mathbf{r}_{CM,k}(t_i)$ is the mass center of the k th IVC which has n_k atoms and is calculated by taking the average of each atom inside.

The concurrent ESCM coupling requires an iteration process between the MD and FEM domain. The displacements of the atoms at the MD/FE Interface are calculated by taking a statistical average over the atomic positions in each IVC and are averaged again over the time steps being taken for the MD process. The average displacements are then applied onto the FE domain as the displacement boundary conditions, which can be written as δ_l . After the finite element analysis, the reaction force R_l are obtained from the interface and distributed to the atoms in the IVC as the traction boundary condition for the MD system. A stable equilibrium of both displacement and forces between the continuum and the atomistic domain on the coupling interface will be reached through the coupling iteration of the algorithm. The dynamics of the embedded MD domain can be described by Newton's equations of motion according to Eq.(51) in the previous chapter,

$$\begin{aligned} m_i \mathbf{r}_i &= \mathbf{f}_i & (i \in \text{Inner MD domain}) \\ m_i \mathbf{r}_i &= \mathbf{f}_i + \frac{\mathbf{R}_I^k}{N_I^k} - c \mathbf{v}_{CM}^k & (i \in (\text{IVC})^k \text{ Interface MD domain}) \\ m_i \mathbf{r}_i &= \mathbf{f}_i + \frac{\mathbf{f}_c^k}{N_S^k} - c \mathbf{v}_{CM}^k & (i \in (\text{IVC})^k \text{ Surface MD domain}) \end{aligned} \quad (82)$$

where the subscript i refers to the i^{th} atom, superscript k stands for the k^{th} IVC, c is the phonon damping coefficient to absorb the intense phonon waves coming from a propagating crack, damping \mathbf{R}_I^k is the reaction force on the interface and \mathbf{f}_c^k is the compensating force, which is required to maintain the initial atomic reference states in order to simulate the response of an

infinite molecular system under external forces when coupled with FEM domain. The detail of calculating \mathbf{f}_c^k can be found in 0.

4.2 Anchor points

S. Pfaller *et al.* [12] introduced the so-called anchor points, which are assigned in the coupling region, to transfer information between MD and FE domains. Each anchor point is bonded to a standard MD particle harmonically. The interaction between the I^{th} anchor point is connected to a MD particle through the following harmonic potential

$$E_{A,I}^{\text{int}} = \frac{1}{2} k_I |\mathbf{r}_I^A - \mathbf{R}_I^{\text{MD}}|^2 \quad (83)$$

in which k_I refers to the force constant, \mathbf{r}_I^A is the position of the anchor point and \mathbf{R}_I^{MD} is the current position of the MD particle that is connected to.

By introducing a weighting factor $\alpha (\alpha \in [0,1])$ in order to weight the energies in the respective domains, the energy of the harmonic bonds between anchor points and MD particles can be obtained as

$$E_A^{\text{int}} = \frac{1}{2} \sum_{I=1}^{n_A} [1-\alpha] E_{A,I}^{\text{int}} \quad (84)$$

On the one hand, anchor points provide more flexibility in coupling MD with continuum domain; on the other hand, it allows the coupling scheme to be adjusted through the coupling parameters in order to match with the real material behavior.

4.3 Modified ESCM coupling procedure

In our MPM-MD coupling scheme, the so-called ‘‘anchor point’’ approach proposed by S. Pfaller *et al.* [12] is implemented in order to transfer information between continuum and molecular system. The anchor points are added into the original EPON 862 MD model as extra

carbon atoms in the polymer chain as shown in Figure 4.1, and each anchor point is anchored to a fixed position in the coupling domain of MPM cells for every MD time step, and its new position is updated at the end of each continuum step based on the position of neighboring material points. An appropriate number of anchor points (red points) are created inside the “handshake region” between MD and MPM. Each anchor point is connected to an atom on the polymer chains using a harmonic potential which can be written as

$$\phi(\mathbf{r}, \mathbf{r}_0) = \frac{k}{2} (\mathbf{r} - \mathbf{r}_0)^2 \quad (85)$$

So that the force exerted on the anchor point by the MD system will be

$$\mathbf{F}(\mathbf{r}, \mathbf{r}_0) = -\frac{\partial \phi}{\partial \mathbf{r}_0} = k(\mathbf{r} - \mathbf{r}_0) \quad (86)$$

In the equations above, the stiffness k defines the strength of the connection between the anchor point and the constrained atom and, on the other hand, it defines the way that the MD system is constrained to the continuum MPM system. A proper value of k needs to be chosen in order to establish an appropriate connection between MD system and continuum body.

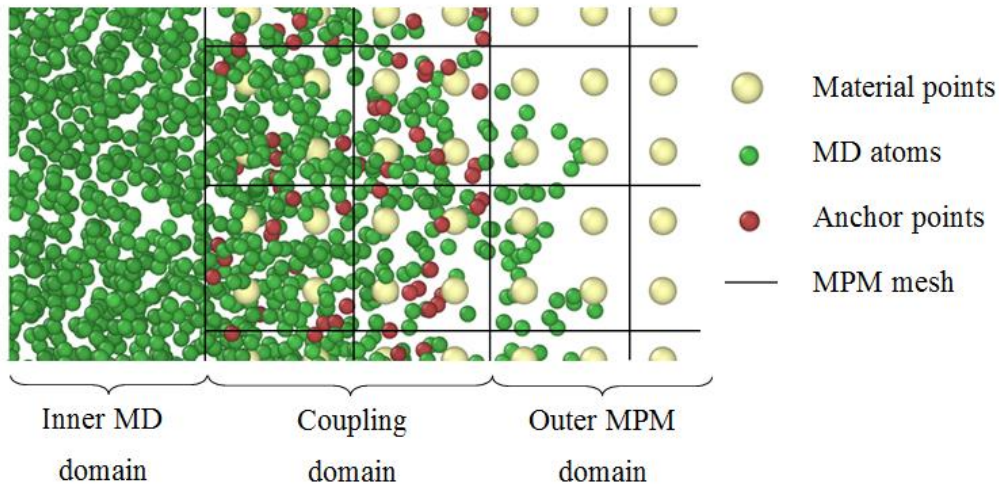


Figure 4.1 MPM-MD coupling system setup

Reaction force from the MD domain is calculated and interpolated onto corresponding material

points. Taking this force as boundary condition for MPM, nodal displacements of the continuum are solved according to standard MPM procedure. The obtained displacements may be interpolated and averaged onto corresponding anchor points. Multiple steps of MD simulations are performed, which then serves as the input for a single step of the continuum simulation. This process is repeated, and in this manner gives rise to an $M:1$ temporal coupling for the concurrent simulation, that is, M MD time steps are equivalent to a single continuum step.

The detailed coupling flowchart is shown in Figure 4.2. and is described below.

1. Initialization

After the MD system with anchor points is equilibrated at the correct temperature and set up for coupling runs, the MPM domain is initialized by the specified far-field boundary conditions and interface forces in coupling zone.

2. MPM-MD coupling iteration

The MPM solver solves Newtonian equations on grid nodes using information interpolated from the material points and, similarly nodal variables, like displacement, velocity and acceleration, are obtained at each continuum time step. Displacements at the anchor points are interpolated from the nodal displacement solutions, which are generated by the MPM solver at the end of the continuum time step.

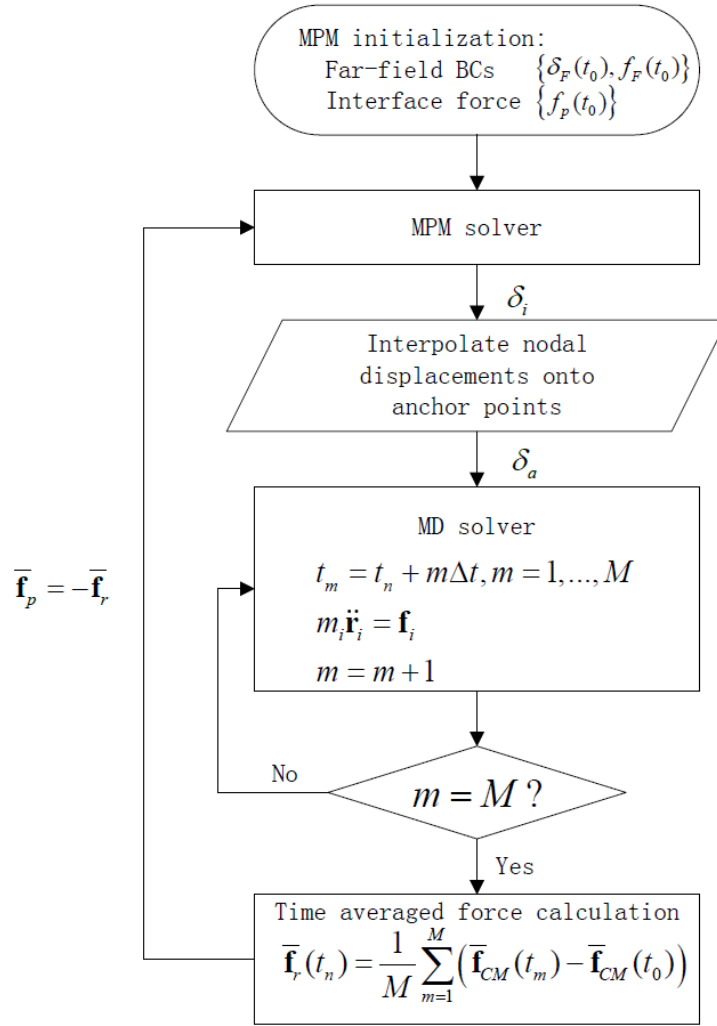


Figure 4.2 Flowchart of MPM-MD coupling procedure

At this point, the MD simulation is initiated with updated anchor point coordinates calculated from interpolated displacements provided from MPM nodal data in the coupling domain. The MD solver is then made to run M time steps for each continuum update of the anchor point positions in order to obtain an $M:1$ temporal coupling and to obtain a well equilibrated state of the MD system. The coupling domain is subdivided into internal volume cells or IVCs as depicted in Fig. 4. Within each IVC the atomic reaction forces for each cell, $\bar{\mathbf{f}}_{CM}$, on the mass

center due to displacement of the anchor points, will be calculated by performing an averaging operation over the atoms within the cell. Then be averaged over the M MD time steps to yield the time-averaged reaction force at each anchor point, $\bar{\mathbf{f}}_r$.

$$\bar{\mathbf{f}}_r(t_n) = \frac{1}{M} \sum_{m=1}^M (\bar{\mathbf{f}}_{CM}(t_m) - \bar{\mathbf{f}}_{CM}(t_0)) \quad (87)$$

where, $\bar{\mathbf{f}}_r$ is the time averaged reaction forces on anchor points, M is the user specified number of MD steps for each MPM step, $\bar{\mathbf{f}}_{CM}$ is the equivalent force on the internal volume cell center mass. This reaction force is equally transmitted to the material points residing within the IVC (refer to Fig. 4) as force boundary condition for the continuum solver. The MPM-MD concurrent coupling iterations continue until the given time criterion is reached.

4.4 Model application: crack modeling in MD-MPM

As the objective of this paper is to develop a way to simulate fracture in a compact tension specimen (CT specimen) with dimensions in inches, concurrently coupled multiscale MPM/MD modeling is imperative to obtain a tractable solution. For the continuum domain, a pre-crack is modeled using CRAMP, which is introduced by J. A. Nairn and Y. Guo [30]. The pre-crack tip is located in the MPM domain outside of the MD zone. This concurrent multiscale modeling approach has flexibility in terms of crack modeling and propagation due to the fact that the crack tip can be created either outside or inside the MD domain. In the former case, the given critical energy release rate is required for the crack to propagate inside the continuum domain; while the latter one assumes pre-crack existence in the molecular domain. In this multiscale scheme, the crack is able to propagate from continuum domain into MD domain through the coupling domain when the last grid node in the coupling zone is detached. ReaxFF (Reactive Force Field) potential, a bond order based force field developed by Adri van Duin, *et al.* [31] is implemented

in the molecular dynamics (MD) simulation.

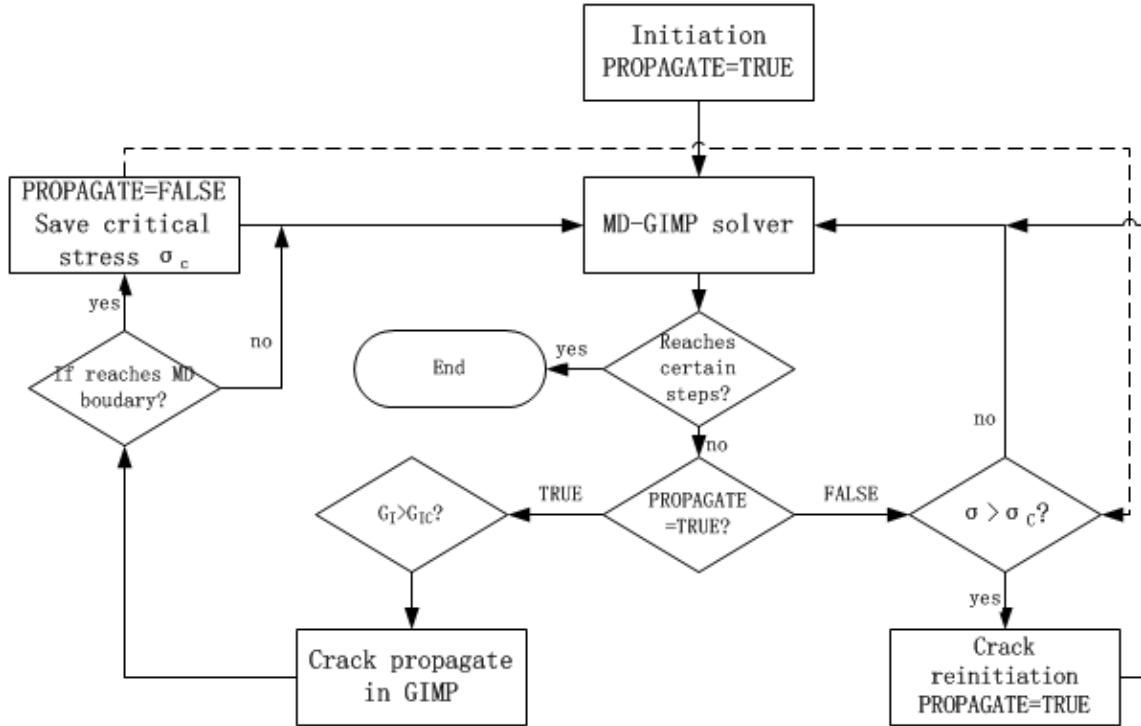


Figure 4.3 Crack propagation process flow chart

The proposed coupling scheme allows big flexibility in crack modeling and the way it propagates. The crack can not only propagate from the continuum into the molecular domain but also from the molecular domain into the continuum. In our approach, the crack can be reinitiated into the continuum zone from MD zone. Figure 4.3 shows the flow chart of this crack propagation process, the GIMP in the chart stands for Generalized Interpolation Material Point method which is a generalized version of MPM and has more flexibility in modeling large deformation problems. In order to achieve this, the critical stress value at the fracture point is

saved and used when crack needs to be reinitiated into the GIMP zone. The detailed crack propagation procedure is shown in Figure 4.3. The dot line indicates the data flow of saved critical stress value. A Boolean variable PROPAGATE is introduced to control the propagation of the crack in GIMP. The fracture inside GIMP is controlled by energy release rate using VCCT and the crack reinitiation into the GIMP is controlled by critical stress saved in the previous GIMP steps. Figure 4.4 shows the time step when crack starts to propagate into the inner MD zone and Figure 4.5 is the time step when crack reinitiates into the GIMP area.

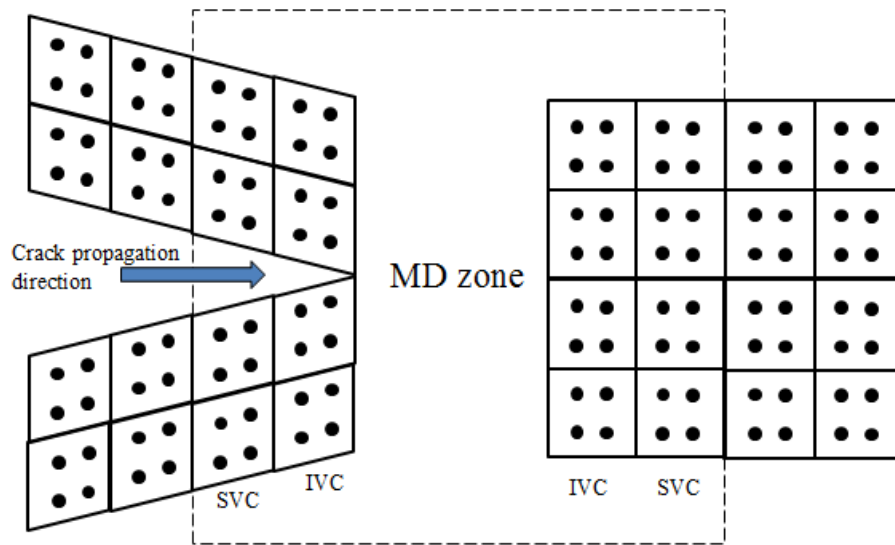


Figure 4.4 Crack begins to propagate into MD zone

In the context of coupling, the MPM code works as the driver program and it calls LAMMPS, which is built as a library, from inside. In LAMMPS, timestepping is performed by the Integrate class within the Update class. The Verlet class is applied in the coupling code in order to perform the Verlet integration algorithm. The following method needs to be called at the beginning of each run:

1. `Imp->init()`: set the internal flags based on user settings.
2. `Imp->setup()`: set up for the running of the method invoke certain fix involved in the simulation.
3. `Imp->force_clear()`: initialize force and other arrays to zero before each timestep.

After calling the methods above, the `Verlet::run()` method can be called. The pseudo code for each run of the `Verlet::run()` method is shown in Figure 4.6. The detailed description of the methods used in Figure 4.6 can be found in the LAMMPS website [53] and related documents [10].

```

ev_set()

fix->initial_integrate()
fix->post_integrate()

nflag = neighbor->decide()
if nflag:
    fix->pre_exchange()
    domain->pbc()
    domain->reset_box()
    comm->setup()
    neighbor->setup_bins()
    comm->exchange()
    comm->borders()
    fix->pre_neighbor()
    neighbor->build()
else
    comm->forward_comm()

force_clear()
fix->pre_force()

pair->compute()
bond->compute()
angle->compute()
dihedral->compute()
improper->compute()
kspace->compute()

comm->reverse_comm()

fix->post_force()
fix->final_integrate()
fix->end_of_step()

if any output on this step: output->write()

```

Figure 4.6 Pseudo code for the Verlet::run() method for each step

CHAPTER 5

RESULTS

As discussed in Chapter 1, the fracture toughness calculated by stress intensity factor K or energy release rate G is not a constant material property but changing with the crack length of the specimen. Based on Eq.(1), the critical crack length, a_c , for graphene is 0.382 nm and for EPON 862 it is 2560nm. Therefore, the fracture model for EPON 862 needs to include a crack which is more than 2560nm to be able to simulate crack initiation and growth. A compact tension loading case of graphene with the size of more than 4000nm is simulated to validate the proposed MPM-MD coupling approach and the ability to model the material in large scale using MPM mesh refinement technique while retaining the length scale characteristic of atomic bond breakage. To our knowledge, this has not been attempted for polymeric material.

5.1 Model benchmark: crack propagation of graphene

The study of crack propagation in a graphene sheet is selected as a benchmark case to validate the MPM-MD coupling model described above. The MD model for graphene contains 4200 atoms and 1968 anchor points are added in the handshake zone of the model. The MPM-MD coupling model is set up as shown in Figure 5.1. The size of the three-dimensional MD domain is $52\text{\AA} \times 52\text{\AA} \times 52\text{\AA}$ which is embedded into a $40960\text{\AA} \times 40960\text{\AA}$ two-dimensional MPM model. The coupling domain or handshake zone of MPM and MD is 15\AA in width and all the anchor points are located within this region. The MPM mesh refinement method discussed previously is applied here to create the coupling model and the continuum domain is built with 10 levels of

meshes varying from 2560\AA to 10\AA in grid size (not shown in Fig. 6 due to resolution issues). The pre-crack length for this case is 19982\AA .

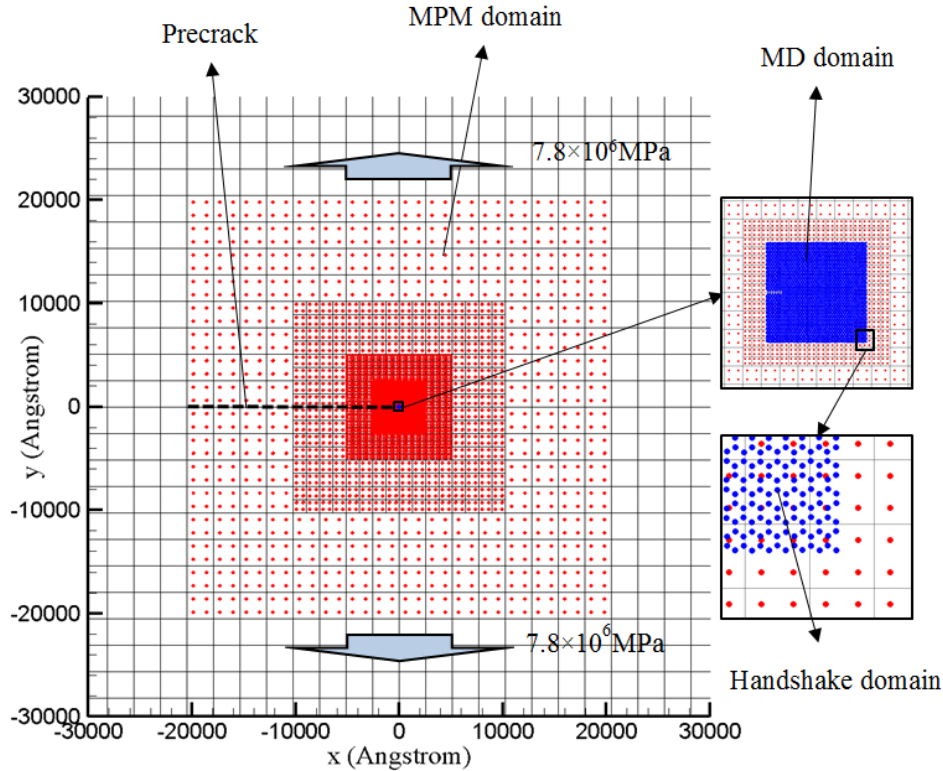


Figure 5.1 MPM-MD coupling model configuration

The material properties of graphene used in the MPM model is as follows: density $\rho=2.0\text{g/cm}^2$, Young's modulus $E=1\text{TPa}$, Poisson's ratio $\mu=0.17$. A uniformly distributed pressure is added on top and bottom of the MPM model as the boundary condition.

The simulation was performed at 300K using NVT ensemble. Zooming in at the crack tip, we are able to observe the propagation for the crack at molecular level (MD) as shown in Figure 5.2 (a)-(d). The figure shows the initiation and propagation of the crack tip in the MD domain from 0fs to 1200fs , during which time the crack extends about 40\AA . Stress concentration can be seen at the atoms around the crack tip and it moves with the tip. The simulation shows the behavior of

a dominant mode I crack in the middle of the model with graphene chains bridging the crack surface as presented in Figure 5.2 (d) and supported by experimental observations in [32].

Unlike linear elastic fracture mechanics, the integral provides a way to calculate the strain energy release rate even when nonlinearities, such as crack bridging, are present near the crack tip, and it is defined as

$$J = \int_{\partial\Omega} (\Psi \mathbf{N} - \mathbf{H}^T \mathbf{P} \mathbf{N}) dA \quad (88)$$

where $\mathbf{H} = \mathbf{F} - \mathbf{I}$ is the displacement gradient tensor, Ψ is the Helmholtz free energy density and \mathbf{N} is the outward normal vector to the surface $\partial\Omega$ enclosing the region Ω . By choosing a square contour around the crack tip in the MD domain, the J-integral value can be estimated numerically as described in [7]. Using this approach, the J values versus time history were plotted as shown in Figure 5.3.

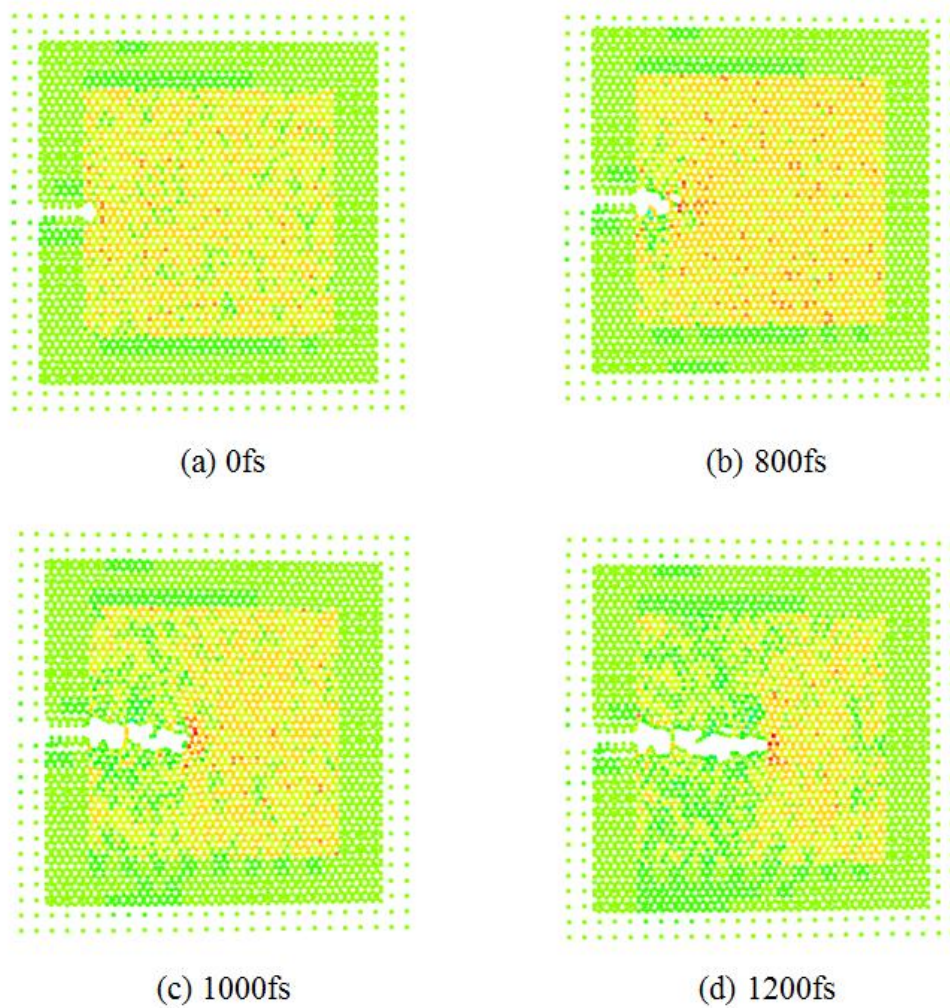


Figure 5.2 Crack propagation in MD domain in a single graphene sheet

As shown from the plot, the energy release rate at the crack tip stays at a relatively low value before the crack propagates, which is depicted in point (a). The J value starts to increase quickly when the crack propagates from (b) to (d), it reaches more than 20 J/m^2 at 1000 fs (c) and then drops down to around 12 J/m^2 after 1100 fs. The sudden increase and subsequent decline in the value of the J -integral are attributable to the formation and breakage of graphene chains bridging the crack. The experimentally measured critical energy release rate for graphene is 16 J/m^2 and the results obtained from the coupling simulation are in good agreement with measured value.

Therefore, the proposed concurrent coupling approach is able to simulate the crack propagation problem in graphene and hence it can be applied to other crystalline material as well.

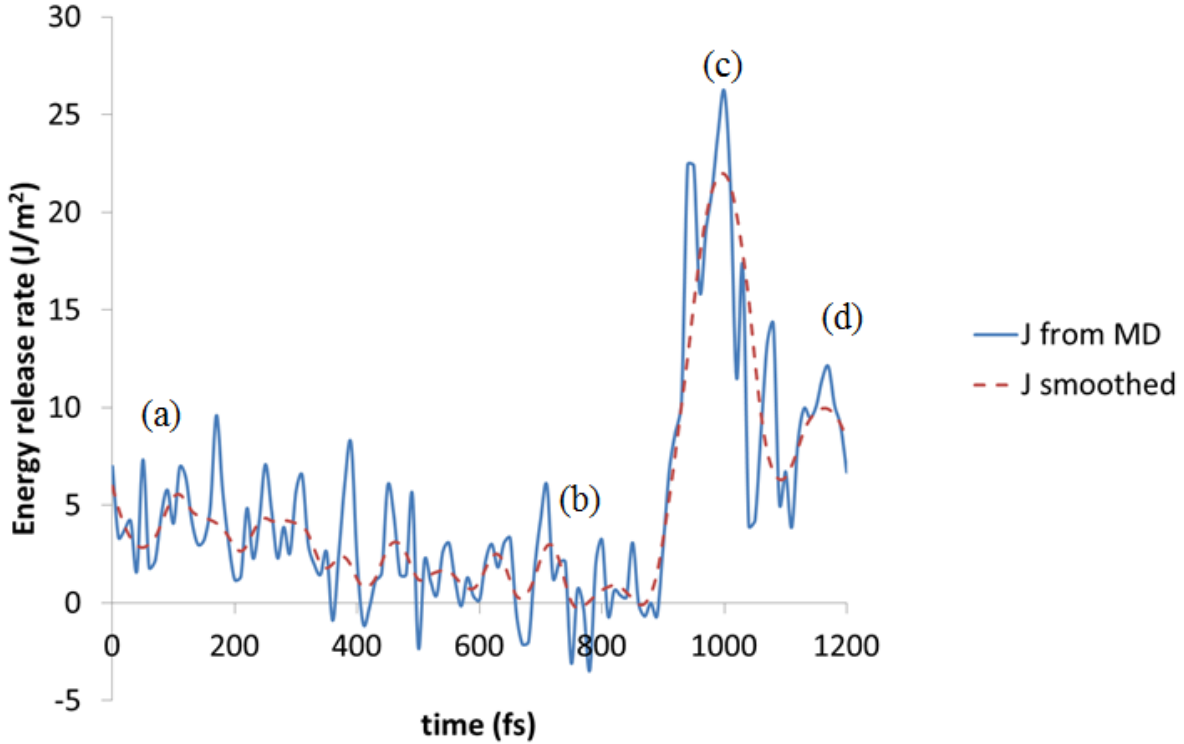


Figure 5.3 J-integral vs. time plot

5.2 Crack propagation of cross-linking polymers

The ultimate goal of this research is to simulate the fracture behavior of large-molecule materials like polymers and predict fracture parameters in polymer-matrix nanocomposite materials. For this purpose, fracture of thermoset epoxy EPON 862 with a 76% crosslink density was simulated using concurrent coupling. The MD model contains 17928 atoms and 962 anchor points in the coupling domain. The number of anchor points is deliberately kept low so that the addition of extra carbon atoms to the polymer chain does not have deleterious effect on the original system. The MPM-MD coupling model for the polymer has a similar configuration as

shown in Figure 5.1. Based on results obtained from Eq.(1) for EPON 862 polymer ($a_c= 2560$ nm), the size of the three-dimensional MD domain for this case is $60\text{\AA}\times 60\text{\AA}\times 60\text{\AA}$ and it is embedded into a $61440\text{\AA}\times 61440\text{\AA}$ two-dimensional MPM model. The handshake zone of MPM and MD is 10\AA in width and all the anchor points are located within this area. The pre-crack length for this case is 31440\AA , which is more than the critical crack length 25600\AA .

The properties for MPM model in this case is as follows: density $\rho=1.3\text{g/cm}^2$, Young's modulus $E=2.258\text{GPa}$, Poisson's ratio $\mu=0.359$.

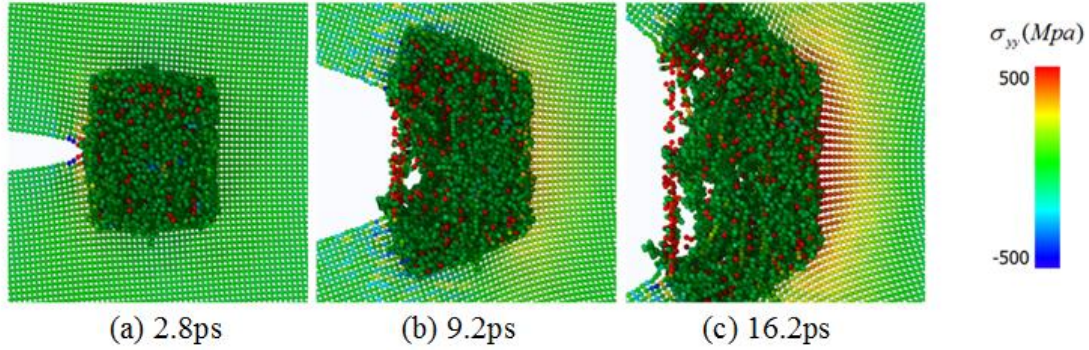


Figure 5.4 Crack propagation in MD domain for EPON 862

The simulation is performed at 300K and NVT ensemble is used for the whole process to keep the temperature constant. Time step size for MPM is 0.1fs and time step for MD is 0.01fs, which means for each continuum step there are 10 MD steps ($M=10$). In this manner, MD system could be equilibrated relatively sufficiently while keeping MPM from wasting unnecessary steps. The crack is initiated from the MPM zone using CRAMP algorithm with VCCT method to calculate energy release rate [19]. In this procedure, the crack tip node is released when the critical energy release rate is reached at a certain continuum time step. When the crack travels into coupling zone, crack begins to propagate through the MD domain and stretches the polymer chains of which two ends located on two sides of the crack edge, as shown

in Figure 5.4(c). As can be seen from Figure 5.4, the crack does not propagate into the polymer due to the formation of a damage zone near the crack tip. Work is underway to study this effect further, and also to calculate the J-integral for this case.

5.3 Problems and future work

The value for energy release rate and toughness obtained from coupling simulations are much lower than the actual value ($G_{Ic}=325\text{J/m}^2$, $K_{Ic}=1.0\text{MPa}\times\text{m}^{1/2}$). The reason for this discrepancy might be from unrealistic stress distribution in MD region. Multiple simulations on stress propagation in crystalline and amorphous material also show evidence that stress wave propagation inside amorphous material cannot be so easily achieved as crystalline materials. The local residual stress is much higher and fluctuate more in amorphous materials comparing with crystalline materials with ordered atomic structure.

The focus of future research needs to address developing a GIMP-ReaxFF coupling for amorphous polymers. The problem of stress wave propagation through the transition region and energy balance between the continuum and atomistic domains during crack growth simulation will require further study. According to Akepati's work [55], the current set of parameters used in the ReaxFF potential for epoxy polymers does not seem to be particularly suitable for fracture simulation, so that a better parameter set needs to be developed so that the simulated fracture process is representative of the actual physical phenomenon. In this manner, it should be feasible to simulate fracture and actually predict the fracture toughness in nano-graphene reinforced polymers. .

CHAPTER 6

HIERARCHICAL MULTISCALE SIMULATION OF OPEN HOLE TENSION TEST FOR A COMPOSITE LAMINATE USING MAC/GMC

This chapter provides a case study of using hierarchically-coupled nano-micro-macro scale simulation of an open-hole tension test of a carbon/epoxy composite laminate, with and without randomly dispersed nano-graphene reinforcements in the polymer matrix. The matrix stiffness and failure properties, with and without nanographene reinforcement, are obtained from MD simulations that were performed in a prior research [56]. These data are then provided as input to the micromechanical model (MAC/GMC) to obtain individual (fiber/matrix) failure modes, as well as stress amplification due to material heterogeneity. Finally, the micromechanical model provides stiffness data, before and after damage has initiated, to the macroscale continuum model (e.g., Finite Element Analysis). Hence, progressive failure in a composite laminate is modeled using this iterative procedure.

6.1 Micro-scale modeling using MAC/GMC

In the NASA developed software, Micromechanics Analysis Code based on the Generalized Method of Cells (MAC/GMC) [57], the repeating volume element, RVE of the periodic composite is identified, and the macroscopic or average stress and strain state in terms of the individual microscopic (subcell) stress and strain states is defined as below.

The average stress in a subcell is given by:

$$\bar{\sigma} = \mathbf{B}^* (\bar{\epsilon} - \bar{\epsilon}^p - \boldsymbol{\alpha}^* \Delta T) \quad (89)$$

where, \mathbf{B}^* is the effective elastic stiffness tensor, $\bar{\boldsymbol{\varepsilon}}$ is the average composite total strain, $\bar{\boldsymbol{\varepsilon}}^p$ is the average composite plastic strain and $\boldsymbol{\alpha}^*$ is the effective coefficient of thermal expansion. For two-dimensional case, where a number of $N_\beta \times N_\gamma$ subcells are defined, \mathbf{B}^* can be given in terms of the subcell stiffness $\mathbf{C}^{(\beta\gamma)}$ and the subcell strain concentration matrices $\mathbf{A}^{(\beta\gamma)}$,

$$\mathbf{B}^* = \frac{1}{hl} \sum_{\beta=1}^{N_\beta} \sum_{\gamma=1}^{N_\gamma} h_\beta l_\gamma \mathbf{C}^{(\beta\gamma)} \mathbf{A}^{(\beta\gamma)} \quad (90)$$

A detailed description of GMC analysis can be found in [47] and [48].

The micromechanics theories localize to the subcell level, and the damage models of MAC/GMC for the constituents can be applied. The nonlinearity resulted from local effects in the fiber or matrix constituents in the structure will be captured and homogenized, thus, their effects can be represented in the macro level. MAC/GMC has the capability of performing failure and damage analysis with varying levels of complexity. The failure criterion can be estimated from the stress and strain allowable data of the constituent materials. Static failure analysis, which constantly checks user specified failure criteria on either the RUC or subcell level, can be applied during the simulation.

In this dissertation, the fibers and matrix are modeled as subcells separately. The Static failure analysis, which is based on the local stress and strain fields in the subcells, is performed during the simulations. In this manner, the specified failure initiation criteria for both fiber and matrix will be checked during the simulated loading history. Subcell failure criteria are used at the RUC level in this work. Maximum strain criterion is used for fiber subcell and maximum stress criterion is used for matrix subcells. The subcell elimination method, wherein the stiffness of the subcell is instantaneously reduced upon failure initiation, is chosen to simulate the damage resulted from subcell failure.

MAC/GMC is able to link with the ABAQUS commercial finite element package to enable linear and nonlinear analysis of composite structures using micromechanics to simulate the fiber and matrix behavior throughout the structure. NASA developed the FEAMAC code to integrate the MAC/GMC within the ABAQUS software package. FEAMAC calls a MAC/GMC library at each FEA step and applies the properties or parameters at the integration point on the element focused on in order to enable the analysis of composite structures. Figure 6.1 shows a RUC model for a Carbon fiber/Nanoparticle reinforced polymer composite (NRPC) composite which has a 2×2 subcell layup which is used in the numerical examples discussed in the following sections. The material properties required as input for the NRPC matrix in MAC/GMC is obtained from prior MD simulations performed by a fellow graduate student

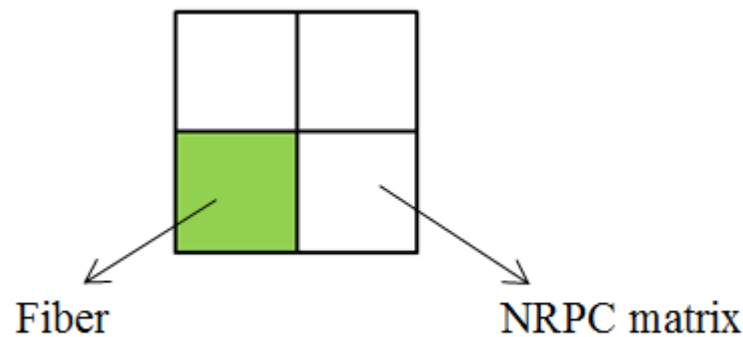


Figure 6.1 RUC model for IM 7/NRPC composite

6.2 Progressive failure modeling of delamination using cohesive zone in FEA

Interlaminar delamination damage is simulated by placing cohesive elements, COH3D8, at potential delamination interfaces in ABAQUS. The constitutive response of the cohesive element

in single-mode loading is defined by a bi-linear traction-separation law. For single-mode loading, the bi-linear cohesive law can be expressed as:

$$\sigma = \begin{cases} K\delta, & \delta < \delta_i \\ (1-d^*)K\delta, & \delta_i \leq \delta < \delta_f \end{cases} \quad (91)$$

where K is the stiffness parameter of the cohesive element, δ is the separation distance, and the damage variable d^* is a function of the displacement jump and accounts for the reduction in the load-carrying ability of the material as a result of damage. The damage variable d^* has a value of zero when the interface is undamaged and a value of one when interface is fully separated.

For mixed-mode crack growth, the onset of delamination is determined based on the quadratic interaction criterion

$$\left(\frac{\langle \sigma_{zz} \rangle}{Y_t} \right)^2 + \left(\frac{\tau_{xz}}{S} \right)^2 + \left(\frac{\tau_{yz}}{S} \right)^2 = 1 \quad (92)$$

The Macaulay bracket $\langle \rangle$ indicates that a compressive normal stress σ_{zz} does not contribute to the damage initiation, while Y_t and S are the interfacial normal and shear strength, respectively. The critical fracture energy for mixed mode failure is determined from the Benzeggagh and Kenane criterion (BK law) [49]:

$$G_c = G_{IC} + (G_{IIC} - G_{IC}) \left(\frac{G_{II} + G_{III}}{G_I + G_{II} + G_{III}} \right)^\alpha \quad (93)$$

where α is the BK material parameter.

6.3 Fracture of open hole composite laminates

Extensive open hole tension experiments for composite laminates was performed by Green *et al.* [50]. The quasi-isotropic laminates of Hexcel IM7/8552 carbon/epoxy prepreg with different

stacking sequences $((45_m/90_m/-45_m/0_m)_{ns})_s$, where m and n are the number of plies of each orientation present, and s signifies a symmetric laminate) were tested in the experiment.

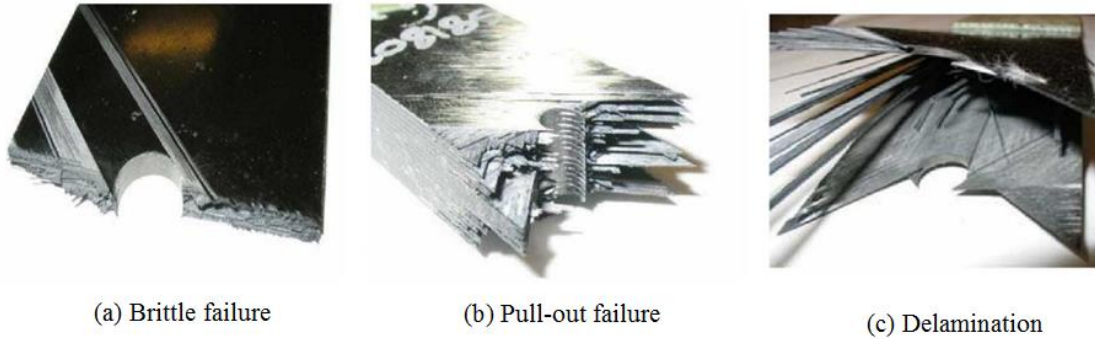


Figure 6.2 Three types of failure mechanisms of laminate ([50])

The experimental investigation suggests the failure of a laminate is not an independent behavior or characteristic of the laminate of a certain layup but the failure stress and mechanism depends on multiple factors like the hole size and thickness of the specimen. Three typical types of failure mechanisms are observed in the tests as shown in Figure 6.2: (a) Brittle failure mode, in which fiber failure is dominant at the fracture surface; (b) Pull-out failure mode, in which delamination and matrix cracking occur on the off-axis plies; (c) Delamination mode, in which delamination is detected extensively at the $-45/0$ interface.

Finite Element Analysis is able to simulate the damage of the material by applying damage criteria on the elements as well as introducing cohesive elements for delamination. However, it becomes extremely difficult to predict the actual failure behavior and failure stress/strain only by making use a “smeared” continuum model of the laminate when the complicated failure mechanism of composite laminate, e.g., fiber fracture and delamination, are present as shown in Figure 6.2. Therefore, it is necessary to apply the hierarchical multiscale modeling method to

accomplish this objective . MAC/GMC provides a way to perform a finite element analysis of the entire test specimen while including subcell damage to the fiber and the matrix at the micromechanical level, through the interrogation of the subcell response at each FEA integration point. Moreover, with the help of the cohesive element of FEM to simulate interlaminar damage, the delamination mode can also be captured in the OHT MAC/GMC-FEA (or FEAMAC) simulation.

6.4 Three-dimensional ply-level analysis using finite element modeling

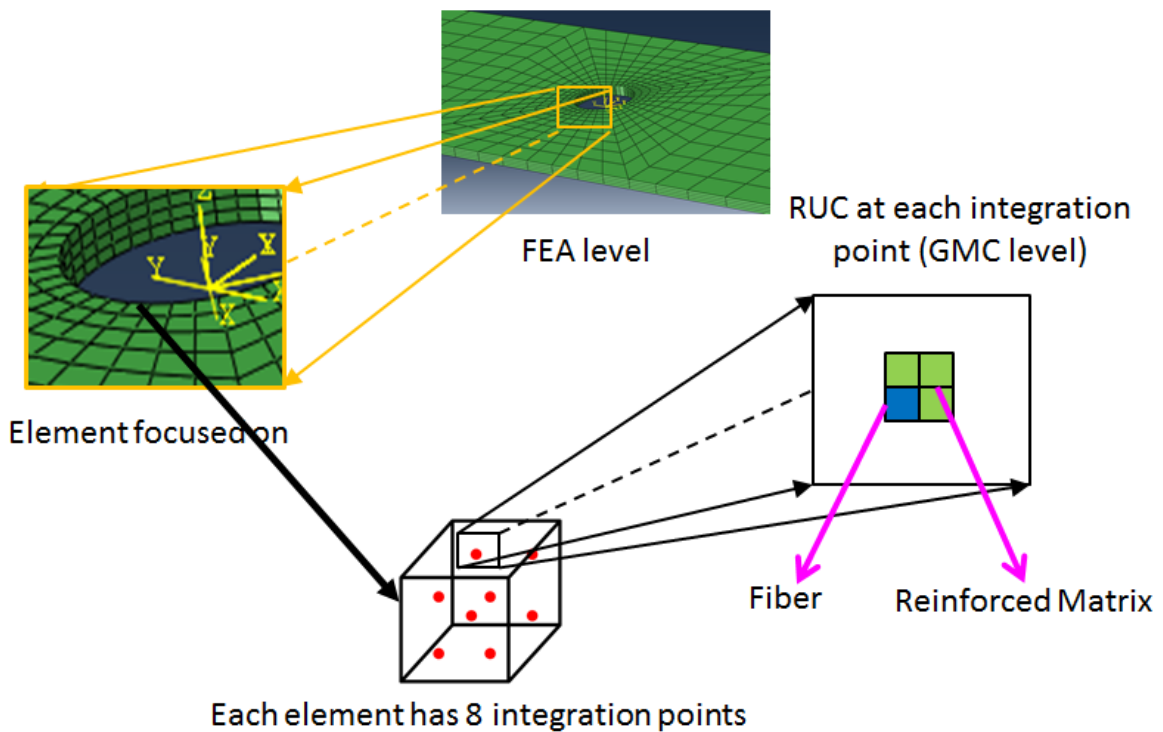


Figure 6.3 Micro-macro coupling (MAC-GMC/Abaqus)

As mentioned earlier, data obtained from lower length scale calculations (i.e., MD) were fed into the hierarchical repeating unit cell (RUC) based multiscale model of nanoparticle reinforced composites (MAC/GMC), which in turn fed into the macroscale FEA model (ABAQUS).

A very effective example of the hierarchical coupling methodology is Abaqus/MAC-GMC coupling for modeling fiber reinforced nano-composites. FEAMAC subroutine developed by NASA acts as a gateway between macro scale (Abaqus) and micro scale (MAC/GMC) for coupled simulation with iterations. Fig 6.3 schematically depicts this flow of information. At each time step of a macro-scale simulation, stresses are computed at each FEA integration point, which is then transferred onto the MAC/GMC model, which in turn calculates local micromechanical stresses based on the constitutive definition acquired from the nano scale. Any damage initiation due to stress amplification at the microscale subcell level results in the degradation of the subcell effective stiffness properties, \mathbf{B}^* , and is passed onto the next macro scale timestep. The resulting change in element stiffness due to microscale damage results in a stress redistribution at the macro-scale for a given applied loading. The new stress state is passed onto the micro-scale and the process is repeated iteratively to predict progression of damage with each time step, all the way to the ultimate failure of the structure.

6.5 Case study: Simulation of an Open Hole Tension experiment using hierarchical multi-scale modeling

In the following simulations, nano scale stiffness and damage parameters for unreinforced (neat resin) and graphene reinforced EPON 862 (NGP aspect ratio= 2 NGP wt%= 2%) were obtained from MD simulations published in a prior work by a student in Dr. Roy's group [56]. To incorporate the properties in the micro scale GMC, the stiffness parameters were homogenized assuming a random orientation of the nano graphene in the EPON 862 matrix. The homogenized properties were then incorporated in a 2×2 RUC model in GMC as in Figure 6.1. Damage at the micro scale was modeled using a critical stress-based approach for the matrix subcell, and a critical strain based approach for the fiber subcell. The strength estimates for the

matrix subcell were directly obtained from MD simulations. In the following sections, two case studies are presented where the OHT experiment is simulated as a demonstration of the capabilities of hierarchical multi-scale modeling.

6.5.1 Case study 1: OHT simulation of laminate with $[0/90]_s$ layup

A simple cross-ply $[0/90]_s$ laminate layup was chosen in this case study. Each lamina was made of IM7/EPON862 NRPC (Nano-particle Reinforced Polymer Composite) composite material (60% volume percentage for fiber). The properties of fiber and matrix (with and without nanographene) used as input to the multi-scale model are listed in Table 6.1 and Table 6.2.

Table 6.1 NRPC matrix properties

	Young's modulus (GPa)	Poisson's ratio	Strength (MPa)
neat resin	2.963	0.36	118.67
2wt% NRPC	3.5811	0.36	121.02

Table 6.2 Fiber properties

	Tensile Modulus (GPa)	Poisson's ratio	Tensile Strength (MPa)	Maximum strain(MPa)
IM7 6K fiber	276	0.33	5,515	1.90%

A two-dimensional double periodic RUC model was used to model continuous fiber IM7/NRPC composite material as shown in Figure 6.1. The cell in green represented fiber, and the remaining cells were matrix, whose properties were defined from the above tables. Subcell

failure criteria including maximum strain and stress criterion were incorporated into the model to simulate micro-scale failure behavior for open hole tension test.

Using symmetry, only a 1/8 FEA model was created, and symmetry boundary conditions applied as shown in Figure 6.4. The full laminate size was 8mm×8mm with thickness of 1mm (but only half the thickness was modeled in FEA model) and the hole size was 3.175mm in diameter. The FEA model is shown in Figure 6.4 consisting of eight-noded three-dimensional continuum solid elements (C3D8). Each lamina was modeled using a single layer of elements. Uniaxial displacement in the global x-direction was applied on the nodes on one side of the laminate to simulate the tensile test as shown in Figure 6.4.

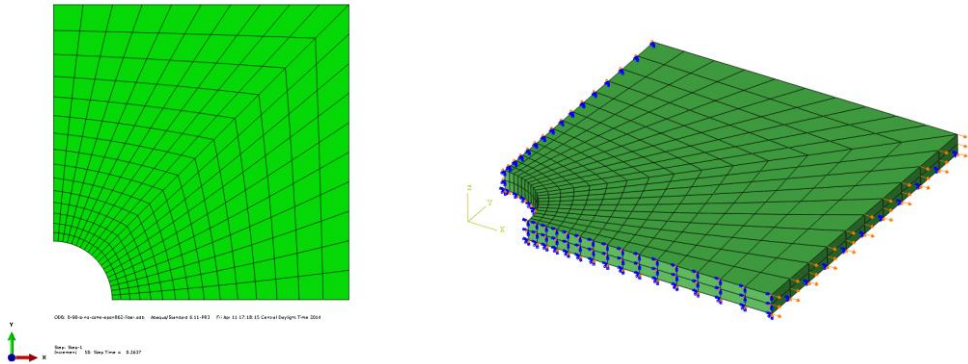


Figure 6.4 FEA model and boundary conditions

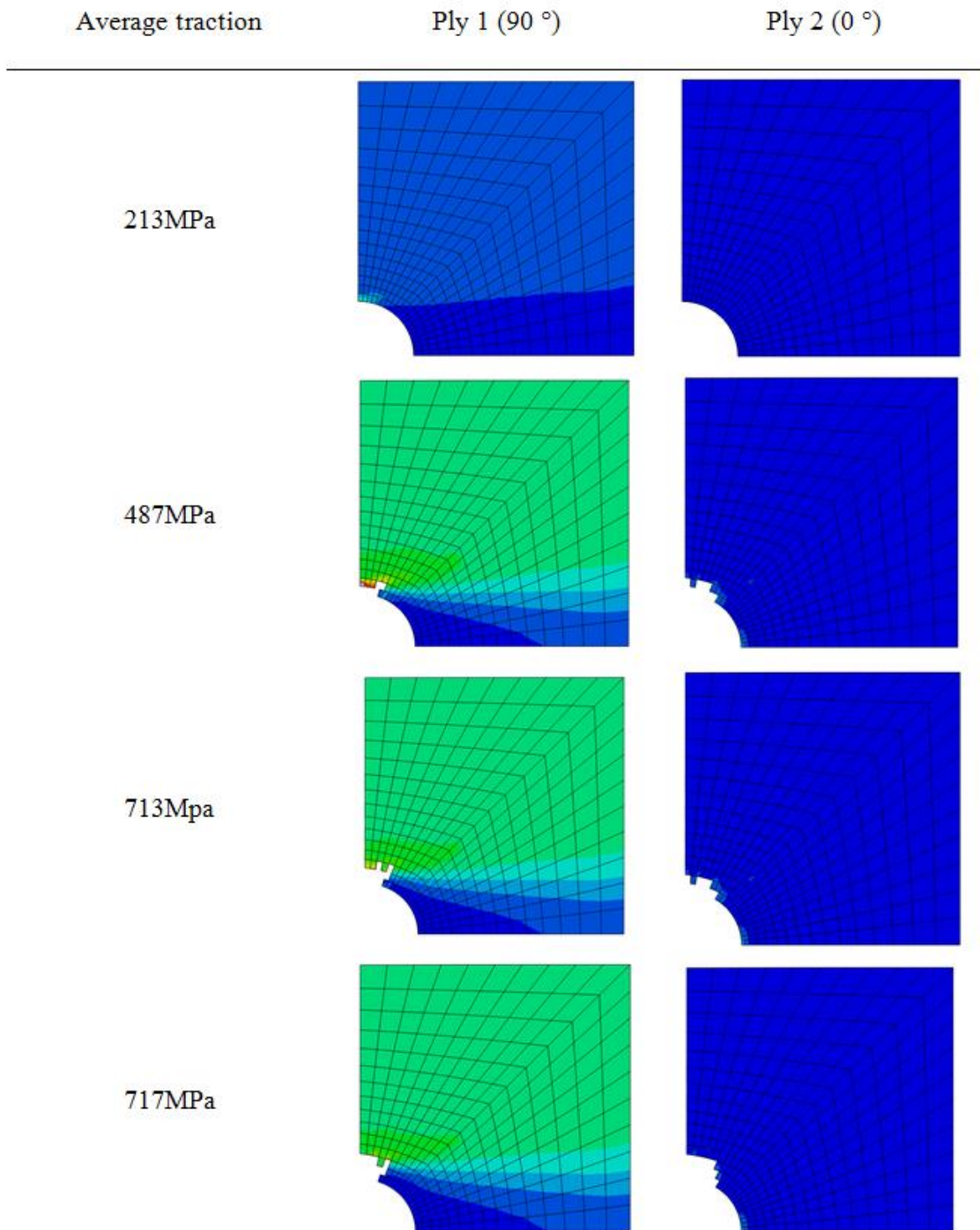


Figure 6.5 Damage prediction of [0/90]_s laminate (2.4%wt graphene)

Average traction was calculated from the reaction forces on nodes on which uniaxial displacement was applied. As the displacement increased, the average traction reached its maximum value and then catastrophic failure occurred shown in Figure 6.6. As listed in Table 6.3, the open hole laminate strength of NRPC with 2 A.R. graphene (2wt%) was increased by only 0.67% compared with neat resin, but the failure strain showed an increase of 4% . Hence, for this case study, the addition of 2wt% of nanographene did not have a significant effect on the open-hole tension strength of the cross-ply laminate, although it did enhance the ductility of the laminate. The likely cause for this lack of strength increase might be because the open-hole tension failure is dominated by fiber fracture rather than matrix cracking. The progressive damage propagation in the laminate is presented as a function of applied load as shown in Figure 6.6.

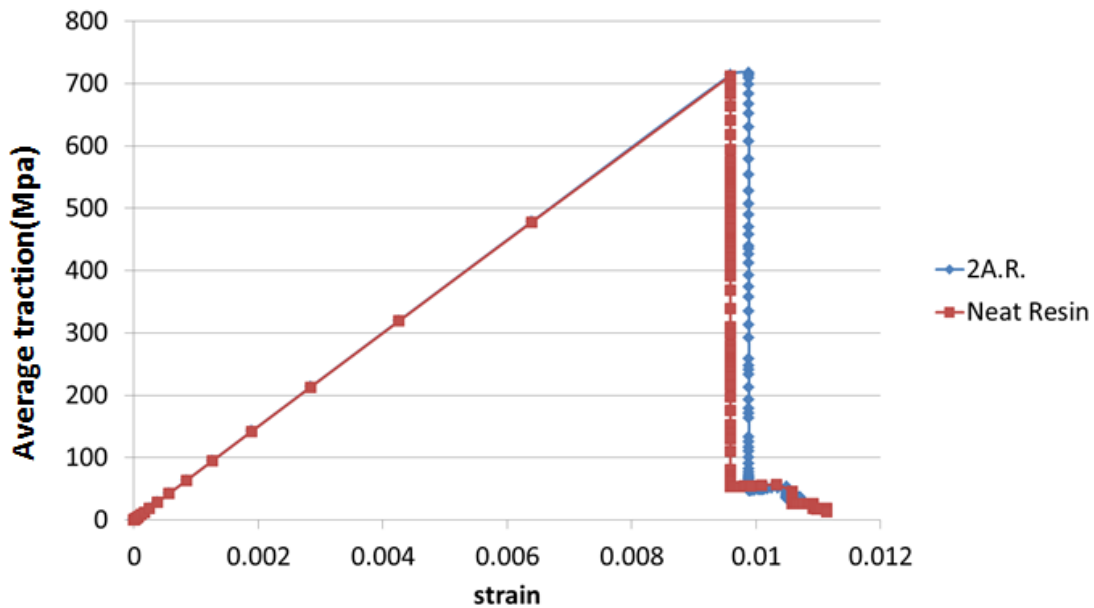


Figure 6.6 Average traction vs. strain plot (Neat resin and 2wt% graphene)

Table 6.3 Strength comparison of neat resin and 2wt% NGP

	Neat Resin	Epoxy with 2wt% NGP
Strength (MPa)	712.30	717.08

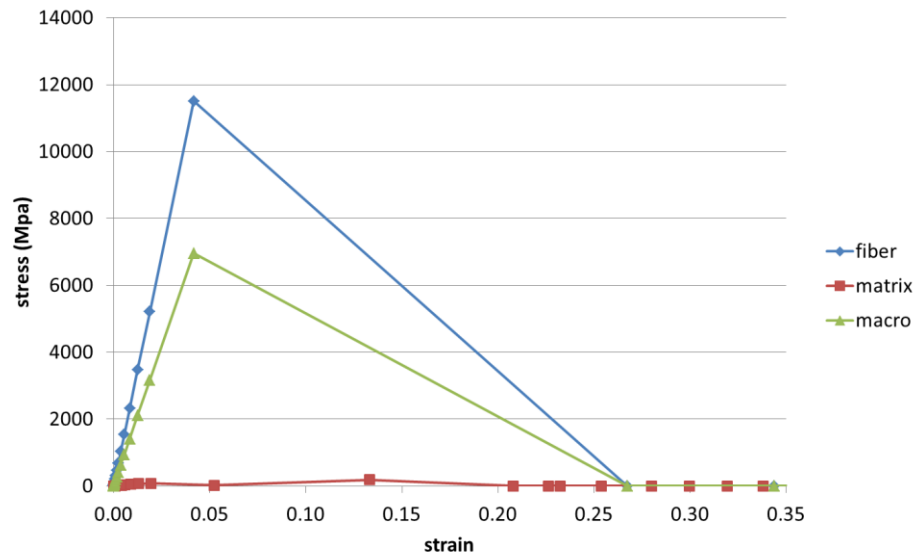


Figure 6.7 Micro and macro stress vs. strain plot of element on 0° lamina (2wt% graphene)

Figure 6.7 and Figure 6.8 show micro (subcell) and macro (finite element) data for element on 0° (tensile direction) and 90° lamina (transverse direction), respectively. Figure 6.7 can be seen as mechanical behavior of subcells in fiber tensile direction and, as depicted from the figure, the carbon fiber carries most of the load for this cell. On the other hand, Figure 6.8 shows the behavior of subcells in transverse direction, and the matrix becomes the more dominant component which carries most of the transverse load.

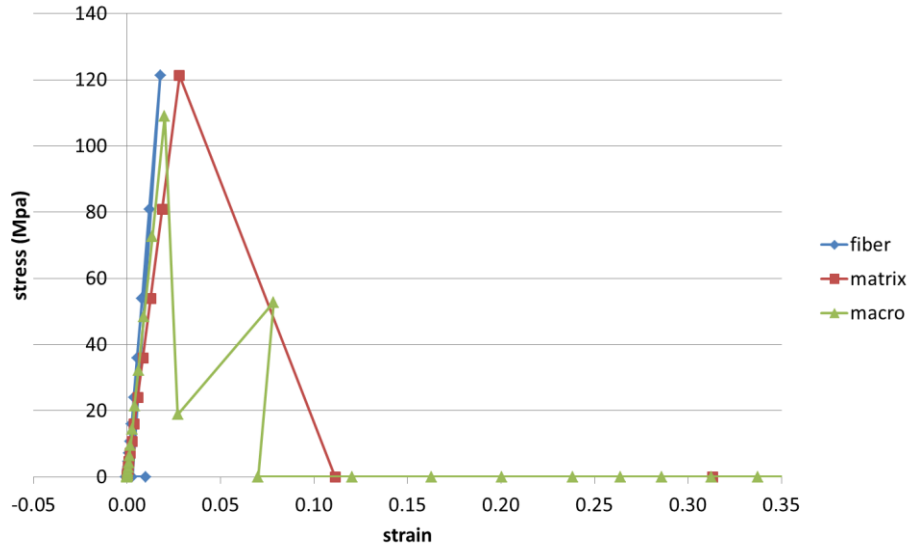


Figure 6.8 Micro and macro stress vs. strain plot of element on 90 °lamina (2w% graphene)

6.5.2 Case study 2: OHT simulation of laminate with [45/0/-45/90]_{2s} layup

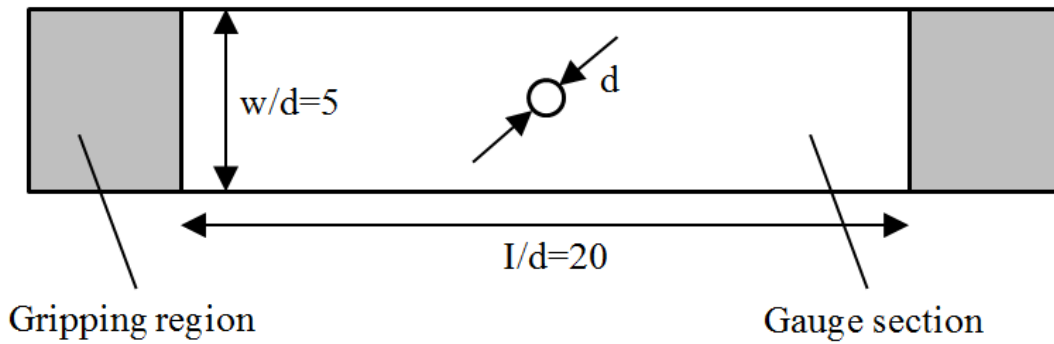


Figure 6.9 Open hole tension specimen geometry

For this case study, a laminate stacking sequence was chosen to be [45/90/-45/0]_s. A schematic of the open-hole tension (OHT) specimen considered is shown in Figure 6.9. Carbon fiber/epoxy prepreg, IM7/Epon862 was used as the material (properties shown in Table 6-4 and

Table 6.5). A specimen hole diameter to width ratio of 5 was chosen because at this width the linear elastic stress concentration should be reduced to the far field stress at the specimen edge. The experimental data indicates that the failure progression and the mode of laminate failure are dependent on the laminate layup (stacking sequence and ply thickness) and the scaling of strength with respect to size is dependent on the type of failure. The basic laminate layup of $[45/90/-45/0]_s$ was studied here using method of multi-scale modeling to test the capability of FEAMAC in solving a practical problem.

Table 6-4 IM7 Fiber properties

Young's modulus (Axial) (MPa)	276000
Young's modulus (Transverse) (MPa)	7600
Maximum strain	1.90%
Tensile strength (MPa)	5655
Shear strength (MPa)	134
Poisson's ratio	0.3

Table 6.5 Epon862 matrix properties

Young's modulus (MPa)	2577
Maximum strain	1.70%
Tensile strength (MPa)	120
Shear strength (MPa)	80
Poisson's ratio	0.32

As in the prior case study, each individual ply of the laminate was modeled using eight-noded solid brick elements in Abaqus (C3D8), was compatible with FEAMAC. Cohesive layers were inserted between plies and were modeled using COH3D8 zero-thickness cohesive elements. A total of 3920 elements were used. The properties of the cohesive zone are shown in Table 6.6, where the variables are defined in section 6.2.

Table 6.6 cohesive zone properties

K (MPa/mm)	2.71×10^8
G_{IC} (N/mm)	0.2
G_{IIC} (N/mm)	1
σ_I^{Max} (MPa)	60
σ_{II}^{Max} (MPa)	90
α	1

Figure 6.10 shows an example of an open hole tension (OHT) specimen using the methodology mentioned above. The specimen is a $[45/0/-45/90]_{2s}$ laminate with EPON 862 matrix and IM7 fiber and nano graphene as the nanoscale reinforcement. The laminate size is $64\text{mm} \times 16\text{mm}$ with thickness of 0.5mm and hole size of 3.175mm in diameter.

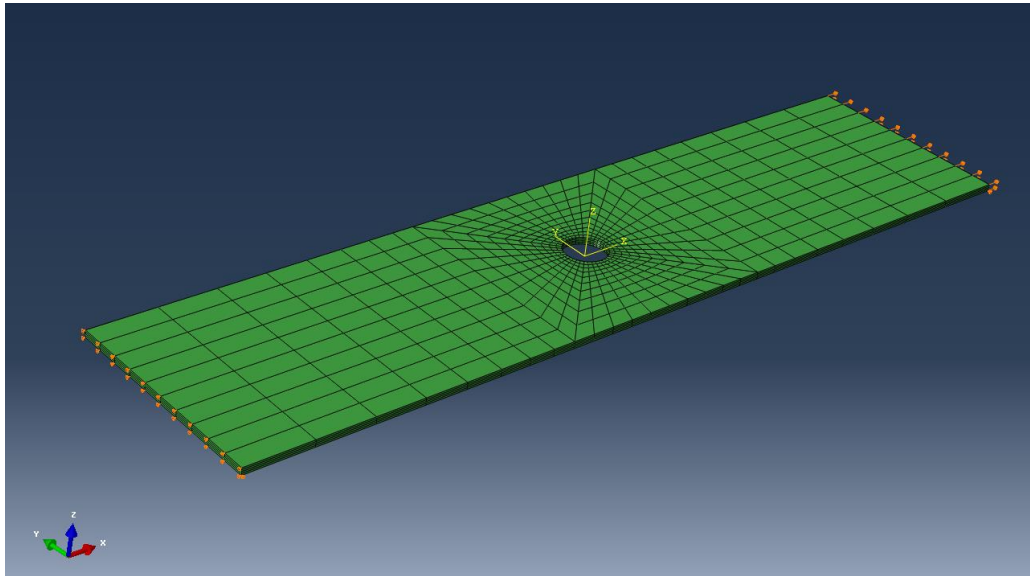


Figure 6.10 OHT FEA model and boundary conditions in laminate

An OHT specimen undergoing tensile loading was modeled in the Abaqus finite element software and was iteratively coupled with GMC to model the microscale RUC. The iterative coupling was not extended to the nanoscale in the interest of computational efficiency. In addition to evolving damage within the RUC, a cohesive damage model available in Abaqus was employed to model macro-scale interlaminar delamination occurring outside the micro-scale RUC. Fig. 6.11 (a) shows the load-displacement plot for the OHT simulation under uniaxial tensile loading at room temperature. Several cases were studied, with and without nanographene reinforcement and delamination modeling, to observe its influence on the predicted failure load. Fig. 6.11 (b) is a magnified view of Fig. 6.11 (a) at the load drop, in order to provide a clearer view of the effects of nanographene and delamination on predicted peak load. As is evident from Figure 6.11, the hierarchical multiscale model is able to capture small changes in stiffness and

failure strength (Figure 6.11(b)), due to the presence of nanographene. It is also evident that while the influence of nanographene platelets is somewhat significant in increasing the OHT strength of the composite, the inclusion of cohesive layers to model inter-ply delamination is not as significant for this case.

Figure 6.12 shows the evolution of von Mises stress contours with applied load (strain) in each individual lamina until maximum load is reached. Based on Figures 6.11 and 6.12, the specimen failure is catastrophic and occurs due to the failure of the load bearing fibers in the 0° layer once the failure strain is reached. For this simple example as shown in Fig. 6.11, the hierarchical multi-scale model predicts a 3.7% increase in OHT strength over baseline case with the addition of 2wt% of NGP (with platelet aspect ratio (AR) = 2) if delamination was not modeled using cohesive elements between lamina. The model predicts a 4.1% increase in OHT strength over baseline case with the addition of 2wt% NGP (with platelet AR = 2) if delamination was modeled using cohesive elements between lamina. The load-displacement curve for a multi-scale model without damage (green line) is included as a reference.

Hence, the three-level multiscale model predicts a slight increase in OHT strength of the laminate due to the presence of 2wt% NGP in EPON 862 matrix. It should be noted that the unrealistic average aspect ratio of 2 for the NGP was selected in order to keep the number of atoms in the MD simulations tractable. Also, the multiscale failure predictions in Figure 6.11 and Figure 6.11 have not yet been verified using actual OHT experiments.

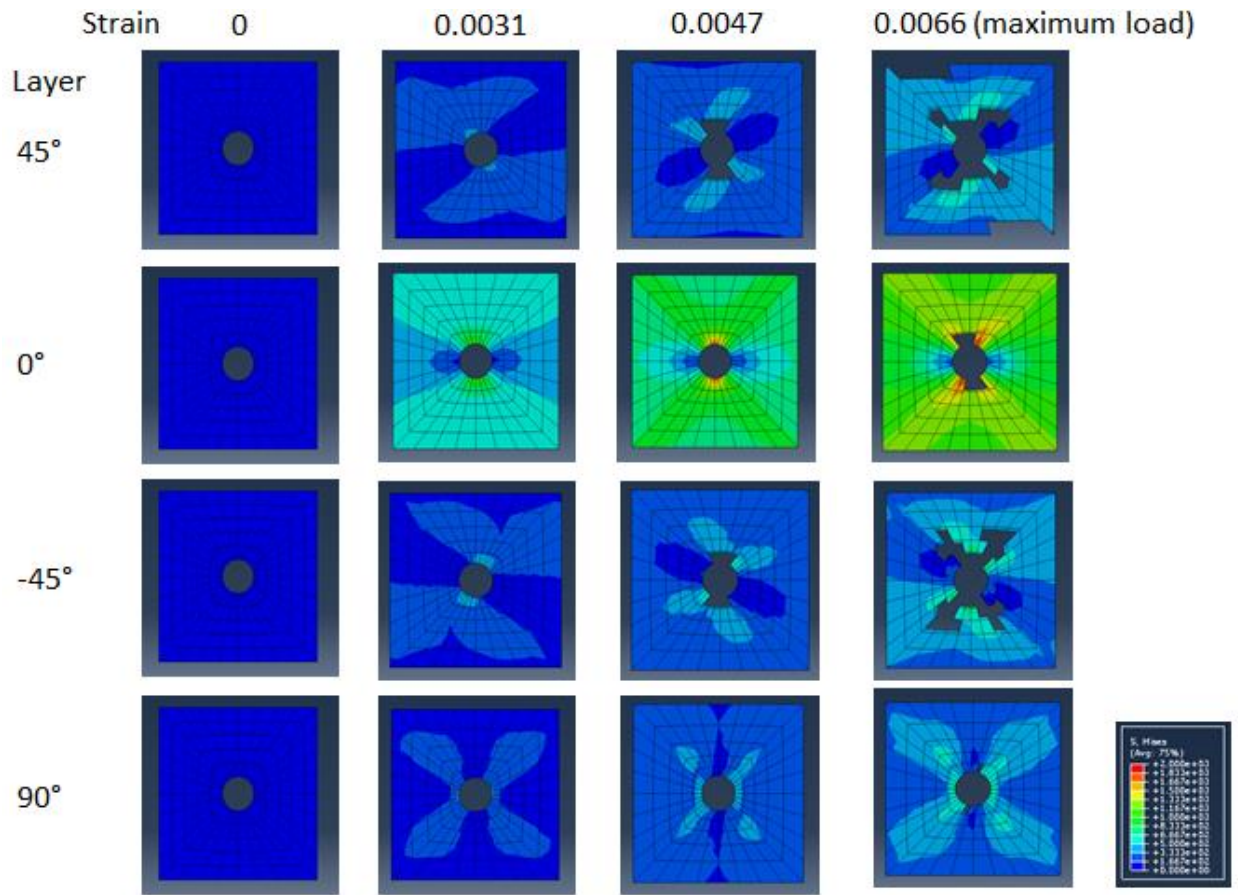


Figure 6.11 IM7/ Reinforced EPON 862 OHT simulation-stress contour for individual lamina as a function of applied strain

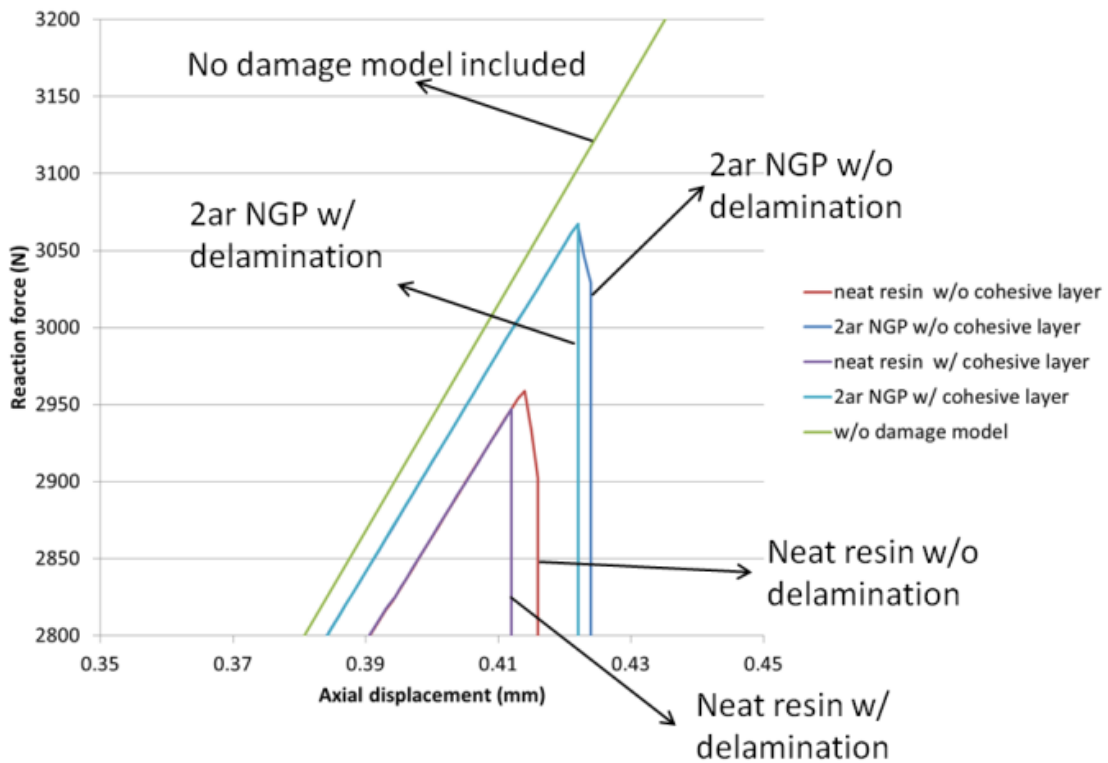
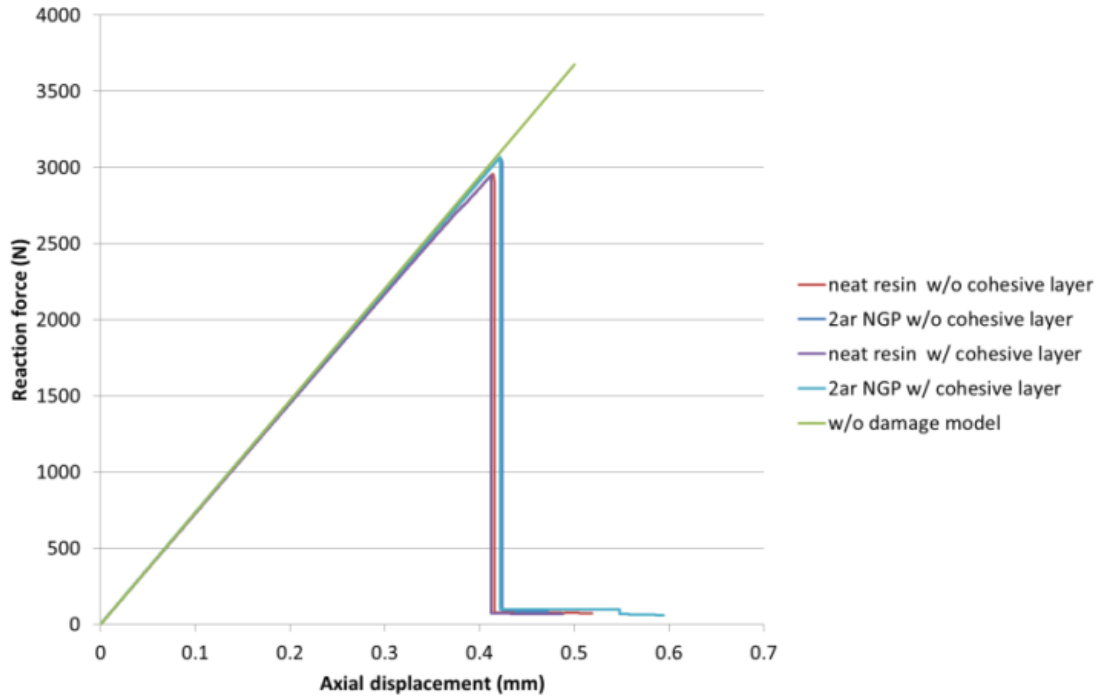


Figure 6.12 (a) Load displacement plot for multiscale OHT simulation for various cases (b) Magnified view at load drop

6.6 Summary and discussion

The results in the previous section show the capability of hierarchical multiscale modeling to simulate the open hole tension failure of a composite laminate. The multiscale modeling approach is able to simulate the brittle failure and delamination by making use of the subcell failure criterion and the cohesive element, however, it does not capture the pull-out mode as discussed in Section 6.3. The proposed model has limitations in modeling all the failure mechanisms of OHT for the reason that MAC/GMC is based on the modeling of subcells and interacts with FEM through the integration points of the element, so that, it becomes challenging when more complicated damage mode is involved like the multiple failure modes in OHT problems. Additionally, the analysis presented is basic and by no means exhaustive. Complex damage mechanisms at the micro scale can be modeled derived from the nano scale fracture and strength based damage mechanisms. The example follows a smooth framework with a simple damage process, but it could become computationally expensive if a very large structure has to be analyzed. This problem can be alleviated by allocating only the parts of the model that are subject to high stresses and more likely to fail to be subjected to the full three-level multiscale modeling, which would help in speeding up the computational process.

Concurrent coupling simulation of cross-linked epoxy in continuum and molecular dynamic scale is studied in this work. We focus on the research of the concurrently coupled MPM-MD simulation of nanoscale fracture behavior inside the polymer. A new coupling scheme, which makes use of defined anchor points and statistical calculation of coupling variables, is proposed in this work. Anchor points, the equilibrium positions of the constrained particles, which are designed to transmit displacements and forces between nanoscale and macroscale model, are

defined in the handshake region. The atom-escaping problem is solved by adjusting the way in which variables are transferred and, by combining ESCM with anchor-point method, we find a more promising way to couple the macro scale and nano scale. A concurrently coupled MPM-MD simulation of nanoscale crack propagation inside a di-functional cross-linked thermoset polymer, EPON 862, is performed to verify this new coupling approach, and provide a better understanding of the fracture mechanisms at nanoscale to predict the macro-scale fracture toughness of polymer system. OPLS based on harmonic force field works well for evaluating mechanical properties, however, it is not able to form or break bonds in simulation. Therefore, ReaxFF, which is a bond order based force field and allows for continuous bond formation/breaking, would be a better choice in this case. The energy transfer between MPM and MD has not been fully studied and it is what we will be focusing on in the future study.

The dissertation work has also studied that it is possible to concurrently couple continuum (MPM or GIMP) with the microscale MAC/GMC. From theoretical point of view, we need to change the original stiffness tensor to the effective elastic stiffness tensor which can be obtained from GMC and call failure criterion in the GIMP cycles on each material point to couple MPM with GMC. However, from technical concept, additional work may be required to call the GMC FORTRAN libraries inside MPM which is a C++ code. Both codes may need some changes to be compatible with each other, and uplink and downlink interfaces codes may have to be implemented.

REFERENCES

- [1] A. Kumar, S. Li, S. Roy, JA King, GM Odegard, Fracture properties of nanographene reinforced EPON 862 thermoset polymer system, *Composite Science and Technology*, 114 (7), 2015
- [2] S. Roy and A. Nair, Concurrent Multi-scale Modeling of Nano-Particle Reinforced Polymers using Statistical Coupling of MD and GIMPM, *Proceedings of the 52nd AIAASDM Conference*, 2011.
- [3] R. Miller, E. B. Tadmor, R. Phillipsz and M. Ortizx, Quasicontinuum simulation of fracture at the atomic scale, *Modelling Simul. Mater. Sci. Eng.*, 607–638, 1998.
- [4] J. Knap and M. Ortiz, An analysis of the quasicontinuum method, *J. Mech. Phys. Solids*, 49, pp. 1899–1923, 2001.
- [5] T.Belytschko and S.P.Xiao, Coupling Methods for Continuum Model with Molecular Model, *International Journal for Multiscale Computational Engineering*, 1 (1), 2003.
- [6] Saether, E., Yamakov, V. and Glaessgen, E. H., An embedded statistical method for coupling molecular dynamics and finite element analyses, *Int. J. Numer. Meth. Engng*, 78 (11), 1292–1319, 2009.
- [7] R. E. Jones, J. A. Zimmerman, J. Oswald and T. Belytschko, An atomistic J-integral at finite temperature based on Hardy estimates of continuum fields, *Journal of Physics: Condensed Matter*, 23, 2011.
- [8] S. Roy and A. Akepati, Multi-Scale Modeling of Fracture Properties for Nano-Particle Reinforced Polymers Using Atomistic J-Integral, *ASME 2014 International Mechanical Engineering Congress and Exposition*, 2014.
- [9] R. Hardy, Formulas for determining local properties in molecular dynamics simulations: shock waves, *Journal of Chemical Physics*, 76(1), pp. 622-628, 1982.
- [10] S. Plimpton, Fast Parallel Algorithms for Short-Range Molecular Dynamics, *J Comp Phys*, 117, 1-19, 1995.
- [11] Cheng, S. and Sun, C., Size-Dependent Fracture Toughness of Nanoscale Structures: Crack-Tip Stress Approach in Molecular Dynamics, *J. Nanomech. Micromech*, 10.1061/(ASCE) NM.2153-5477.0000063, A4014001, 2014.

- [12] S. Pfaller, M. Rahimi, G. Possart, P. Steinmann, F. Müller-Plathe, M.C. Böhm, An Arlequin-based method to couple molecular dynamics and finite element simulations of amorphous polymers and nanocomposites, *Computer Methods in Applied Mechanics and Engineering*, 260, 109-129, 2013.
- [13] Honglai Tan and John A. Nairn, Hierarchical, Adaptive, Material Point Method for Dynamic Energy Release Rate Calculations, *Comput. Methods Appl. Mech. Engrg*, 191, 2095-2109, 2002.
- [14] J. Ma, H. Lu, B. Wang, S. Roy, R. Hornung, A. Wissink and R. Komanduri, Multiscale Simulations Using Generalized Interpolation Material Point (MPM) Method And SAMRAI Parallel Processing, *CMES*, 8(2), pp. 135-152, 2005.
- [15] J. Ma and R. Komanduri, Structured Mesh Refinement in Generalized Interpolation Material Point (MPM) Method for Simulation of Dynamic Problems, *CMES*, 12(3), pp. 214-227, 2006.
- [16] Sulsky D., Chen Z., and Schreyer, A particle method for history-dependent materials, *Computer Methods in Applied Mechanics and Engineering*, 118:179–196, 1994.
- [17] S.G.Bardenhagen and E.M.Kober, The Generalized Interpolation Material Point Method, *Computer Modeling in Engineering & Sciences*, 5, 477-495, 2004.
- [18] John A. Nairn and Yajun Guo, Material Point Method Calculations with Explicit Cracks, *Modeling in Eng. & Sci.*, 4 (6), 649-664, 2003.
- [19] Krueger, R, Virtual crack closure technique: History, approach, and applications, *Appl Mech Rev*, 57 (2), 109-143, 2004.
- [20] Y. GUO and J. A. NAIRN, Calculation of J-Integral and Stress Intensity Factors using the Material Point Method, *CMES*, 1-14, 2004.
- [21] Irving, J. H., Kirkwood, J. G., The statistical mechanical theory of transport processes, IV, The equations of hydrodynamics, *J. Chem. Phys*, 18, 817-829, 1950.
- [22] Cormier, J., Rickman, J. M., Delph, T. J., Stress calculation in atomistic simulations of perfect and imperfect solids, *J. Appl. Phys.*, 89, 99-104, 2001.
- [23] Lutsko, J. F., Stress and elastic constants in anisotropic solids: molecular dynamics techniques, *J. Appl. Phys.*, 64, 1152-1154, 1988.
- [24] Arun K. Subramaniyan, C.T. Sun, Continuum interpretation of virial stress in molecular simulations, *International Journal of Solids and Structures*, 45, 4340-4346, 2008.

- [25] Samit Roy and Abilash Nair, Multiscale Modeling of Nano-Particle Reinforced Composites using Statistical Coupling of MD and MPM, AIAA, 2010.
- [26] H. Lu, N. P. Daphalapurkar, B. Wang, S. Roy, R. Komanduri, Multiscale simulation from atomistic to continuum – coupling molecular dynamics (MD) with the material point method (MPM), *Philosophical Magazine*, 86 (20), 2971-2994, 2006.
- [27] Rahimi, Mohammad, Karimi-Varzaneh, Hossein Ali, Böhm, Michael C., Müller-Plathe, Florian, Pfaller, Sebastian, Possart, Gunnar, and Steinmann, Paul, Nonperiodic stochastic boundary conditions for molecular dynamics simulations of materials embedded into a continuum mechanics domain, *The Journal of Chemical Physics*, 2011.
- [28] Zhou, A new look at the atomic level virial stress: on continuum-molecular system equivalence, *Proceedings of the Royal Society of London, A*, 2347–2392, 2003.
- [29] J. A. Zimmerman, E. B. Webb, III, J. J. Hoyt, R. E. Jones, P. A. Klein, D. J. Bammann, Calculation of stress in atomistic simulation, *Modelling and Simulation in Materials Science and Engineering*, 12, S319–S332, 2004.
- [30] John A. Nairn and Yajun Guo, Material Point Method Calculations with Explicit Cracks, *Modeling in Eng. & Sci.*, 4 (6), 649-664, 2003.
- [31] Adri C. T. Van Duin, Siddharth Dasgupta, Francois Lorant, William A Goddard, ReaxFF: A Reactive Force Field for Hydrocarbons, *The Journal of Physical Chemistry A*, 105 (41): 9396–9409, 2001.
- [32] Chuanhong Jin, Haiping Lan, Lianmao Peng, Kazu Suenaga, and Sumio Iijima, Deriving Carbon Atomic Chains from Graphene, *Phys. Rev. Lett.* 102, 205501, 2009.
- [33] Aboudi, J., "Micromechanical Analysis of Composites by the Method of Cells," *Applied Mechanics Reviews*, Vol. 42, pp. 193- 221, 1989.
- [34] Paley, M. & Aboudi, J., Micromechanical analysis of composites by the generalized cells model, *Mechanics of Materials* 14, 127–139, 1992.
- [35] Aboudi, J., Micromechanical analysis of composites by the method of cells - update, *Appl. Mech. Rev* 49(10), S83–S91, 1996.
- [36] J. G. Bennett and K. S. Haberman, An Alternate Unified Approach to the Micromechanical Analysis of Composite Materials, *J. Compos. Mater.*, vol. 30, pp. 1732–1747, 1996.
- [37] B. A. Bednarczyk and M.-J. Pindera, Inelastic Thermal Response of Gr/Cu with Nonuniform Fiber Distribution, *J. Aerospace Eng.*, vol. 9, pp. 93–105, 1996.
- [38] J A Nairn. Material PointMethod Calculations with Explicit Cracks. *Computer Modeling in Engineering and Sciences*, 4(6):649–663, 2003.

- [39] Fermi E., Pasta J., Ulam S.. Studies of nonlinear problems. I., Los Alamos report LA-1940 (1955).
- [40] B. J. Alder, T. E. Wainwright, Studies in Molecular Dynamics. I. General Method. *J. Chem. Phys.* 31 (2): 459, 1959.
- [41] Rahman, A.. Correlations in the Motion of Atoms in Liquid Argon. *Physical Review* 136 (2A): A405–A411, 1964.
- [42] Jorgensen WL, Tirado-Rives J. The OPLS Force Field for Proteins. Energy Minimizations for Crystals of Cyclic Peptides and Crambin. *J. Am. Chem. Soc.* 110 (6): 1657–1666, 1988.
- [43] J. R. Rice, A Path Independent Integral and the Approximate Analysis of Strain Concentration by Notches and Cracks, *Journal of Applied Mechanics*, 35 , pp. 379–386, 1968.
- [44] J. D. Eshelby, The elastic energy-momentum tensor, *Journal of Elasticity*, 5(3), pp 321-335, 1975.
- [45] Hutchinson, J. W., Singular behaviour at the end of a tensile crack in a hardening material, *Journal of the Mechanics and Physics of Solids* 16 (1): 13–31, 1968.
- [46] Rice, J. R.; Rosengren, G. F., Plane strain deformation near a crack tip in a power-law hardening material, *Journal of the Mechanics and Physics of Solids* 16 (1): 1–12, 1968.
- [47] Aboudi, J., *Mechanics of Composite Materials: A Unified Micromechanical Approach*, Elsevier, The Netherlands, 1991.
- [48] Aboudi, J., Constitutive Behavior of Multiphase Metal Matrix Composites with Interfacial Damage by the Generalized Cell Model, in *Damage in Composite Materials*, G. Z. Voyiadjis (Ed.), pp. 3-22. Elsevier, Amsterdam, 1993.
- [49] Benzeggagh, M.L. and Kenane, M.. Measurement of Mixed-mode Delamination Fracture Toughness of Unidirectional Glass-Epoxy Composites with Mixed-mode Bending Apparatus, *Composites Science and Technology* , 56: 439-449, 1996.
- [50] G. G. Green, M. R. Wisnom and S. R. Hallett, An Experimental Investigation Into the Tensile Strength Scaling of Notched Composites, *Composites Part A: Applied Science and Manufacturing*, Vol. 38, No. 3, pp. 867-878, 2007.
- [51] H. Tan and J. A. Nairn, Hierarchical, adaptive, material point method for dynamic energy release rate calculations, *Computer Methods in Applied Mechanics and Engineering*, 191 (19-20):2123–2137, 2002.

- [52] J. Ma, H. Lu, and R. Komanduri, Structured mesh refinement in generalized interpolation material point (GIMP) method for simulation of dynamic problems, *Computer Modeling in Engineering and Sciences*, 12:213–227, 2006.
- [53] <http://lammmps.sandia.gov>.
- [54] MAC/GMC 4.0 User’s Manual-Keywords Manual. NASA/TM-2002-212077/VOL2.
- [55] A. R. Akepati, A methodology for predicting fracture toughness of nano-graphene reinforced polymers using molecular dynamics simulation, Ph.D. Dissertation, The University of Alabama, 2015.
- [56] Samit Roy and Ankit Srivastav, Multiscale Modeling of Progressive Failure in Polymer Nanocomposites Using Nanaoscale Informed Damage Mechanics, *Mechanics of Advanced Materials and Structures*, 2015.
- [57] Bednarczyk, B.A. and Arnold, S.M., MAC/GMC 4.0 User’s Manual – Keywords Manual, NASA/TM-2002-212077/VOL2, NASA Glenn Research Center, Cleveland, OH, 2002.
- [58] S. M. Arnold, Jacob Aboudi, Brett A. Bednarczyk, *Micromechanics of Composite Materials: A Generalized Multiscale Analysis Approach*, Butterworth-Heinemann, 2013.